Title page (Original Research Article)

Characterisation of RNA editing and gene therapy with a compact CRISPR-Cas13 in the retina

Satheesh Kumar[1,2,3], Yi-Wen Hsiao[1], Vickie H Y Wong[4], Deborah Aubin[5,6], Jiang-Hui Wang[1], Leszek Lisowski[7,8,9], Elizabeth P Rakoczy[10], Fan Li[11], Luis Alarcon-Martinez[1,2], Anai Gonzalez-Cordero[5,6], Bang V Bui[4], Guei-Sheung Liu[1,2,3*]

[1]Centre for Eye Research Australia, Royal Victorian Eye and Ear Hospital, East Melbourne, VIC, Australia

[2]Ophthalmology, Department of Surgery, University of Melbourne, East Melbourne, VIC, Australia

[3]Menzies Institute for Medical Research, University of Tasmania, Hobart, TAS, Australia

[4]Department of Optometry and Vision Sciences, University of Melbourne, Parkville, VIC, Australia

[5]School of Medical Sciences, Faculty of Medicine and Health, The University of Sydney, Camperdown, NSW, Australia

[6]Stem Cell Medicine Group, Children's Medical Research Institute, Westmead, NSW, Australia

[7]Translational Vectorology Research Unit, Children's Medical Research Institute, Faculty of Medicine and Health, The University of Sydney, Westmead, NSW, Australia

[8]Military Institute of Medicine, Laboratory of Molecular Oncology and Innovative Therapies, Warsaw, Poland

[9]Australian Genome Therapeutics Centre, Children's Medical Research Institute and Sydney Children's Hospitals Network, Westmead, NSW, Australia

[10]Centre for Ophthalmology and Visual Sciences, University of Western Australia, Perth, WA, Australia

27 [11]Eye Center, Zhongshan City People's Hospital, Zhongshan, Guangdong Province, China

28 *Correspondence and requests for materials should be addressed to

29 Dr Guei-Sheung Liu (rickliu0817@gmail.com). Centre for Eye Research Australia. Address:
30 Level 7, 32 Gisborne Street, East Melbourne, VIC 3002, Australia. Tel: +61399298360.

31

32 Key words: RNA silencing, CRISPR-Cas13, angiogenesis, ocular neovascularization, diabetic
33 retinopathy, gene therapy, retinal organoids

ABSTRACT

CRISPR-Cas gene editing technology has revolutionised the development of novel genetic therapies. CRISPR-Cas13 nucleases are programmable RNA-targeting effectors that can silence gene expression in a reversible manner. Recent iterations of Cas13 nucleases are compact and adequate for adeno-associated virus (AAV) delivery to achieve strong and persistent transduction of various organs in a safe manner. Here, we report significant transcriptomic signatures of Cas13bt3 expression and demonstrate that all-in-one AAV gene therapy with Cas13bt3 can effectively silence *VEGFA* in human retinal organoids and humanised mouse models. Specifically, human embryonic stem cells (hESC)-derived retinal pigment epithelium cells show high expression of Cas13bt3 after virus delivery corresponding to significant reduction of *VEGFA* mRNA. We further show that intravitreal delivery of Cas13bt3 can transduce mouse retinal cells efficiently, reaching the photoreceptor cells for specific knockdown of human *VEGFA*, without impacting mouse *VEGFA* in the trVEGF029 (Kimba) mouse. Our results reveal important considerations for assessing Cas13 activity and establish Cas13bt3 as a potential anti-VEGF agent that can achieve long-term control of VEGF for treatment of diabetic retinopathy and wet age-related macular degeneration.

51 **INTRODUCTION**

52 The emergence of Clustered Regularly Interspaced Short Palindromic Repeats (CRISPR) and
53 CRISPR-associated (Cas) enzymes, known as CRISPR-Cas, has fuelled several gene editing
54 efforts for novel therapeutics in the past decade[1]. Developed by repurposing the bacterial
55 immune defence against phage viruses, CRISPR-Cas harnesses the ability to induce targeted
56 changes to DNA or RNA sequences. Among CRISPR-Cas proteins, CRISPR-Cas13 is of
57 particular interest for its exclusive specificity for RNA. Targeting RNA is especially attractive
58 as it enables control of gene expression without perturbing the genome and introducing
59 permanent changes and is therefore an emerging avenue for therapeutic development[2].

60 Eleven variants of CRISPR-Cas13 have been described to date[3]. Among them, Cas13d
61 (commonly referred to as CasRx) described in 2018 garnered special attention for its compact
62 size of 930aa, making it the first Cas13 enzyme amenable to adeno-associated virus (AAV)
63 delivery. Studies investigating the development of RNA-targeting therapeutics have widely
64 used CasRx to demonstrate preclinical efficacy against disorders affecting vision, hearing and
65 brain function[4, 5, 6, 7], however significant unintended editing have been reported, hampering its
66 clinical progress[8, 9], and the exact specificity profile of CasRx remains contested[10]. More
67 recently, hypercompact Cas13bt3 (also reported as Cas13X) enzymes were described, ranging
68 even smaller at 775aa[11, 12]. The newfound enzyme has been reported to possess high specificity,
69 and its small size enables additional applications such as RNA base editing using a single
70 AAV[13, 14, 15]. The therapeutic potential of Cas13bt3 is yet to be demonstrated, however initial
71 *in vitro* studies show promising efficiency and safety[13, 16].

72 As a leading cause of blindness in the elderly population affecting 200 million people
73 globally, ocular neovascularisation refers to a group of conditions characterised by the
74 abnormal growth of leaky blood vessels in the eye. Vascular endothelial growth factor (VEGF)

75 has been described as a key mediator of this process, and the overexpression of *VEGFA*
76 underlies pathological angiogenesis and neovascularisation in common ocular diseases like
77 diabetic retinopathy (DR) and neovascular age-related macular degeneration (nAMD). Regular
78 (monthly/ bimonthly) administration of anti-VEGF drugs is the approved front-line treatment
79 modality for these patients[17]. Delivered through intravitreal injections, frequent administration
80 of anti-VEGF drugs poses a significant clinical burden on healthcare institutions and patients
81 due to risk of infection, patient anxiety, clinic capacity and availability of trained healthcare
82 personnel among others[18].

83 We have previously described a potential alternative therapy to current anti-VEGF
84 injections using an all-in-one AAV CRISPR-CasRx gene therapy for the treatment of ocular
85 neovascularisation. This approach was validated *in vitro* in HEK293FT and MIO-M1 cells,
86 demonstrating more than 90% and 50% *VEGFA* mRNA knockdown, respectively[19]. Here, we
87 utilize the novel Cas13bt3 to demonstrate potent *VEGFA* knockdown *in vitro* in human cell
88 lines, in 3D human embryonic stem cells (hESC)-derived retinal organoids and *in vivo* in
89 transgenic humanised mouse retinas. Promisingly, our results show significant knockdown of
90 *VEGFA* mRNA in human cell lines without impact on predicted off-target genes. Single cell
91 RNA sequencing (scRNA-seq) was used to characterise Cas13bt3-mediated *VEGFA* mRNA
92 knockdown at single cell resolution in human retinal organoids identifying, for the first time,
93 the overall transcriptomic impact and cell-specific activity of the enzyme. Lastly, *in vivo* gene
94 therapy showed robust *VEGFA* mRNA silencing in mouse models of proliferative diabetic
95 retinopathy along with control of neovascularisation symptoms. These findings support the
96 development of Cas13-mediated ocular gene therapy establishing the clinical potential of
97 Cas13bt3 and offering an alternative treatment to current anti-VEGFA treatments.

98 **RESULTS**

99 **CRISPR-Cas13bt3 can knock down *VEGFA* mRNA in mammalian cells with minimal**
100 **unintended targeting activity.**

101 We used our previously described single guide RNAs (sgRNA) targeting Exon 4 of *VEGFA*
102 [19], to develop our new Cas13bt3 constructs and assess RNA cutting efficiency as well as
103 collateral and off target cleavages (**Figure 1A-D**). Collateral activity is the trans-cleavage by
104 Cas13 enzymes of adjacent mRNA transcripts as the result of an activated nuclease domain
105 (**Figure 1B**). Off-target activity, on the other hand, is the targeting of other non-target mRNA
106 transcripts due to unspecific binding of the sgRNA (**Figure 1C**).

107 We sought to compare and validate efficiency of the new Cas13bt3 enzyme by testing
108 RNA cutting against two previously established RNA-targeting methods, RNA interference
109 (short hairpin RNA, shRNA) and CasRx (a variant of Cas13d). These are widely used for
110 therapeutic and diagnostic applications. The final all-in-one AAV plasmids carrying either
111 *VEGFA*-targeting shRNA or precursor single guide RNA (sgRNA hereafter) with either CasRx
112 or Cas13bt3 (**Figure 1D**) were transfected into HEK293FT cells. Here, to further enhance the
113 expression of Cas13bt3 we incorporated the stronger cytomegalovirus (CMV) promoter instead
114 of the previously used elongation factor 1α short (EFS) promoter.

115 Significant *VEGFA* mRNA knockdown was observed from all three RNA-targeting
116 methods, with up to 70% shRNA *VEGFA* mRNA knockdown ($P < 0.001$), while CasRx and
117 Cas13bt3 achieved up to 90% knockdown ($P < 0.0001$) compared to vector controls (AAV
118 plasmid carrying a fluorescent marker) (**Figure 1F**, n = 4 independent experiments). Next, we
119 sought to determine if the reduction in mRNA would also lead to a decrease in protein levels.
120 Interestingly, ELISAs for VEGFA revealed that only the Cas13bt3 treatment led to significant
121 reduction of VEGFA protein in the cell supernatant (**Figure 1G**, $P < 0.05$; n = 4 independent

experiments). As both Cas13 variants proved potent in silencing *VEGFA* mRNA in HEK293FT cells, we next transfected immortalised human retinal pigment epithelium cells (ARPE19 cell line) with the *VEGFA*-targeting CasRx and Cas13bt3 plasmids and again observed up to 90% knockdown ($P < 0.05$, n = 3 independent experiments) with Cas13bt3 against vector controls (**Figure S1**), suggesting that Cas13bt3 is a promising candidate for RNA silencing of retinal cells.

To further understand transcriptome-wide effects, we performed bulk RNA sequencing (RNA-seq) on HEK293FT cells transfected with shRNA, CasRx and Cas13bt3. RNA-seq was also performed on cells treated with either control, Cas13bt3 only, Cas13bt3NT and Cas13bt3VEGFA constructs to identify collateral and off-target activity of Cas13. Differentially expressed genes (DEGs) were similar for all treated groups, shRNA, CasRx and Cas13bt3 (**Figure S2A-C**), indicating that collateral activity from the new Cas13bt3 is comparable to previously established RNA-targeting methods. Interestingly, the non-targeting (NT) sgRNA group exhibited the highest number of DEGs, a finding that corresponds with recent studies (**Figure 1G, H and S2A-D**) [16, 20]. Volcano plots of Cas13bt3 samples against control demonstrated and confirmed a significant downregulation of *VEGFA* mRNA only on cells that received the VEGFA targeting treatment (**Figure 1I).**

We identified potential off-target genes through NCBI BLAST of our VEGFA sgRNA sequence and studied the expression levels of the top 10 candidate off-target genes (**Figure S3A**). None of the off-target genes were significantly downregulated, indicating lack of off-target activity from Cas13bt3 (**Figure 1J**), as was the case for shRNA and CasRx (**Figure S2F**).

To further examine the varying DEG levels between the NT and targeting sgRNAs, we identified the top significantly enriched gene ontology (GO) terms for the Cas13bt3-NT

146 sgRNA and Cas13bt3-VEGFA sgRNA groups. Top 5 significant GO terms for the Cas13bt3-
147 NT sgRNA group were all positive enrichments and specifically showed upregulation of RNA
148 binding processes, such as "*pre-mRNA binding*" and "*mRNA 3' UTR binding*", possibly
149 explaining the elevated levels of DEGs in this group. On the other hand, with a VEGFA
150 sgRNA, the top 5 GO terms were all negative enrichments and particularly showed
151 downregulation of "*platelet-derived growth factor (PDGF) binding*" and "*PDGF receptor*
152 *binding*", both angiogenesis promoting factors (**Figure 1K**). A recent study showed CasRx to
153 have intrinsic targets that affected essential processes like RNA metabolism and mitotic cell
154 cycle [20] and opined that this could underlie the lethality seen upon CasRx expression in a mouse
155 model [21]. Here, we found laminin-related processes (e.g., "*laminin binding*", "*laminin*
156 *complex*") were strongly downregulated across all groups (Cas13bt3 only, Cas13bt3-NT
157 sgRNA and Cas13bt3-VEGFA sgRNA) suggesting intrinsic targets could exist for Cas13bt3
158 as well (**Extended data** 1).

159 While Cas13bt3 may undergo activation after maturation of a NT sgRNA; without
160 adequate homologous pairing, the catalytic pocket cannot be formed for efficient nuclease
161 activity [22]. On the other hand, with a targeting gRNA, Cas13bt3 would be activated to form the
162 Cas13bt3-gRNA-target complex for targeted knockdown. Our results suggest that with a NT
163 sgRNA, Cas13bt3 initiates an unspecific target-search process involving significant RNA
164 binding that greatly impacts the expression levels of several genes, while a targeting sgRNA
165 narrows the target-search process to reduce overall transcriptomic impact. Notably, despite
166 high levels of overall DEGs, the number of downregulated genes remained similar between the
167 NT sgRNA and VEGFA sgRNA groups suggesting that the NT sgRNA does not induce
168 formation of the catalytic pocket for RNA knockdown, and altered gene expression is
169 predominantly a result of increased RNA binding.

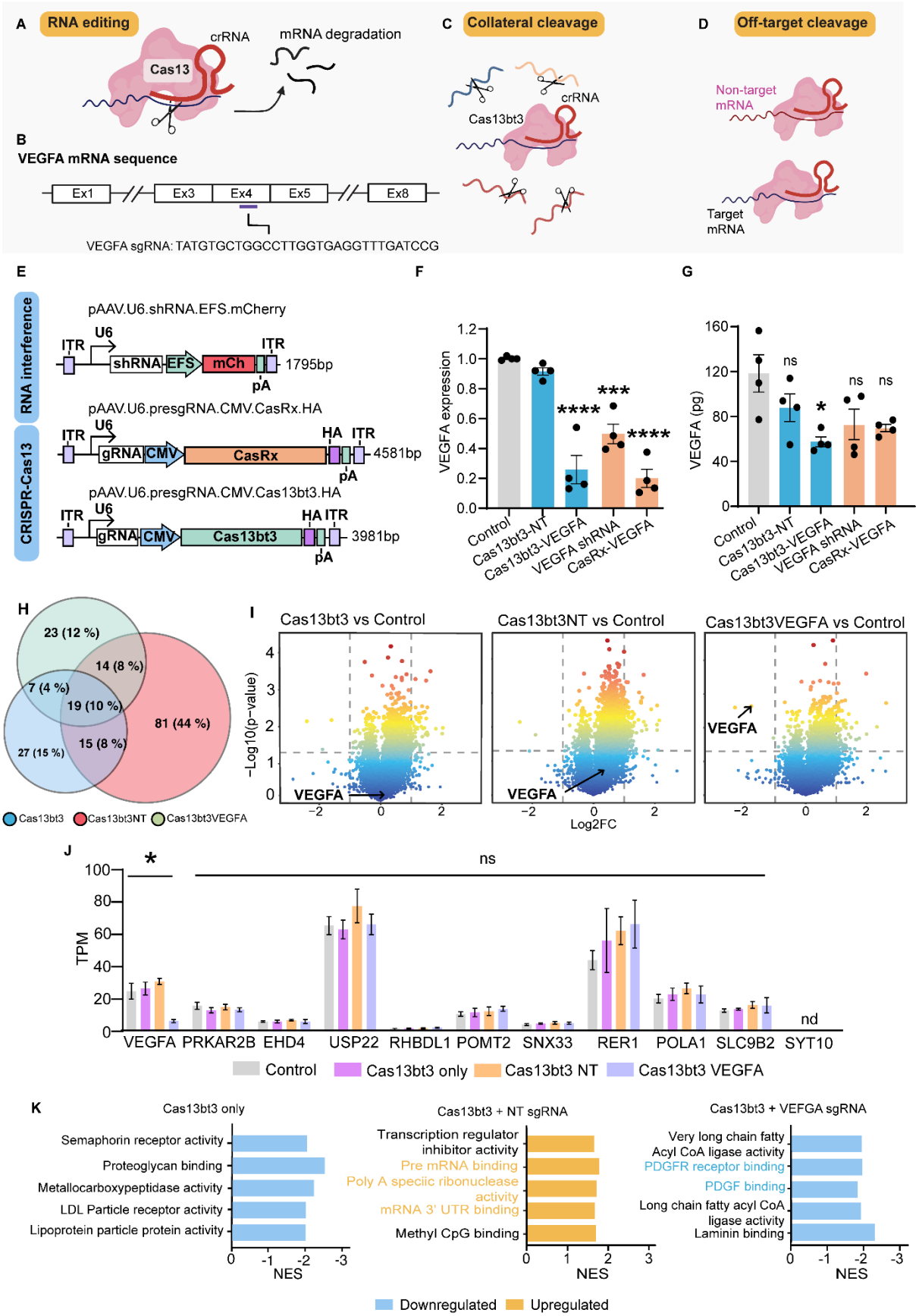
A
RNA editing
crRNA
Cas13
mRNA degradation
B
VEGFA mRNA sequence
Ex1
Ex3
Ex4
Ex5
Ex8
VEGFA sgRNA: TATGTGCTGGCCTTGGTGAGGTTTGATCCG
C
Collateral cleavage
crRNA
Cas13bt3
D
Off-target cleavage
Non-target mRNA
Target mRNA
E
RNA interference
CRISPR-Cas13
pAAV.U6.shRNA.EFS.mCherry
ITR
U6
shRNA
EFS
mCh
ITR
pA
1795bp
pAAV.U6.presgRNA.CMV.CasRx.HA
gRNA
CMV
CasRx
HA
4581bp
pAAV.U6.presgRNA.CMV.Cas13bt3.HA
Cas13bt3
3981bp
F
VEGFA expression
Control
Cas13bt3-NT
Cas13bt3-VEGFA
VEGFA shRNA
CasRx-VEGFA
G
VEGFA (pg)
ns
H
23 (12 %)
14 (8 %)
7 (4 %)
19 (10 %)
81 (44 %)
15 (8 %)
27 (15 %)
Cas13bt3
Cas13bt3NT
Cas13bt3VEGFA
I
Cas13bt3 vs Control
Cas13bt3NT vs Control
Cas13bt3VEGFA vs Control
−Log10(p−value)
Log2FC
VEGFA
J
TPM
ns
nd
VEGFA
PRKAR2B
EHD4
USP22
RHBDL1
POMT2
SNX33
RER1
POLA1
SLC9B2
SYT10
Control
Cas13bt3 only
Cas13bt3 NT
Cas13bt3 VEGFA
K
Cas13bt3 only
Semaphorin receptor activity
Proteoglycan binding
Metallocarboxypeptidase activity
LDL Particle receptor activity
Lipoprotein particle protein activity
NES
Cas13bt3 + NT sgRNA
Transcription regulator inhibitor activity
Pre mRNA binding
Poly A speciic ribonuclease activity
mRNA 3' UTR binding
Methyl CpG binding
Cas13bt3 + VEFGA sgRNA
Very long chain fatty Acyl CoA ligase activity
PDGFR receptor binding
PDGF binding
Long chain fatty acyl CoA ligase activity
Laminin binding
Downregulated
Upregulated

170

171 **Figure 1. Comparison of RNA-targeting tools for in vitro testing of VEGFA mRNA**
172 **silencing. (A)** Schematic of CRISPR-Cas13 mechanism of action. **(B)** VEGFA sgRNA
173 sequence and targeting region on VEGFA mRNA sequence. **(C)** Schematic of collateral and
174 **(D)** off-target cleavage. **(E)** Schematic for domain structure of VEGFA targeting shRNA and
175 Cas13 (CasRx and Cas13bt3) vectors. **(F)** VEGFA mRNA knockdown from shRNA, CasRx
176 and Cas13bt3 in HEK293FT cells (n = 7). **(H)** VEGFA protein expression from ELISA after
177 transfection of shRNA, CasRx and Cas13bt3 plasmids (n = 4). **(F)** Schematic for CRISPR-
178 Cas13 collateral cleavage. **(G)** Venn diagram of total number of differentially expressed genes
179 (DEGs) from Cas13bt3 only, Cas13bt3-NT sgRNA and Cas13bt3-VEGFA sgRNA plasmids.
180 **(I)** Volcano plots showing DEGs from Cas13bt3 only, Cas13bt3-NT sgRNA and Cas13bt3-
181 VEGFA sgRNA compared to transfection control in HEK293FT cells. VEGFA gene is denoted
182 by a black arrow. **(J)** TPM plot for VEGFA and candidate off-target genes. **(K)** Top 5 enriched
183 GO molecular function (MF) terms from Cas13bt3 only, Cas13bt3-NT sgRNA and Cas13bt3
184 VEGFA sgRNA. NES above zero represent significant activation of pathway, while NES
185 below zero represents significant suppression of pathway. Orange text denotes key factors that
186 are upregulated; blue text denotes key factors downregulated. Data presented as mean ± SEM.
187 Statistical analysis was conducted by one-way ANOVA and Tukey's multiple comparison test
188 (**F, G**) and Welch's t-test (**J**). ns: not significant, *P≤0.05, **P≤0.001, ***P≤0.0001,
189 ****P≤0.00001.

190

191

192 **CRISPR-Cas13bt3 sgRNAs multiplexing for knockdown of target gene using a single-**
193 **AAV vector.**

194 The small size of Cas13bt3 and the significant downregulation of *VEGFA* mRNA observed
195 prompted us to hypothesize that multiple sgRNAs can be delivered using a single AAV vector
196 to increase overall targeting and RNA knockdown efficiency. In theory, multiple sgRNAs
197 would increase rate of Cas13 activation and levels of intracellular Cas13-sgRNA complexes
198 for RNA silencing.

199 To understand Cas13bt3 activation and demonstrate multiplex targeting, we transfected
200 Cas13bt3-VEGFA sgRNA and Cas13bt3 with a VEGFA sgRNA array (carrying three
201 VEGFA-targeting sgRNAs) (**Figure 2A-C**). Surprisingly, cells transfected with Cas13bt3-
202 VEGFA sgRNA or Cas13bt3-VEGFA sgRNA array showed similar levels of significant

203 *VEGFA* mRNA knockdown (<90%) (**Figure 2D,** n = 3 independent experiments). We then
204 sought to study collateral and off-target cleavages from the VEGFA sgRNA array system using
205 RNA-seq. Overall DEGs for both single and multiple sgRNA groups when compared to NT
206 control were comparable and suggested minimal collateral activity from the sgRNA array
207 system (**Figure 2E**). Again, we identified top candidate off-target genes for the other *VEGFA*
208 sgRNAs (**Figure S4B and C**) and did not detect any significant off-target activity in these
209 genes by the Cas13bt3-VEGFA sgRNA array system as well (**Figure 2F**). Active Cas13
210 nucleases competing for target mRNA or low levels of *VEGFA* mRNA transcripts may have
211 resulted in the lack of improvement in targeting efficiency, however our results suggest that
212 multiple sgRNAs can be used simultaneously with Cas13bt3 while still avoiding significant
213 collateral activity.

214 Apart from competition for substrate mRNA, it was recently reported that the presence
215 of "UC" sites on the target mRNA may also affect knockdown efficiency, with "UC" sites
216 within 10-20 bases of spacer binding to allow for optimal cleavage (**Figure S3A**)[16]. We found
217 that while sgRNA1 and sgRNA2 had "UC" sites in these optimal regions, sgRNA3 had only
218 one distal "UC" site 40 nucleotides away from spacer binding (**Figure S3B**). While we did not
219 independently test the knockdown efficiency of our sgRNAs, this finding suggests sgRNA 3
220 alone would achieve low levels of RNA knockdown. As no improved knockdown was
221 observed from the VEGFA sgRNA array, we proceeded to investigate Cas13bt3 with a single
222 sgRNA further.

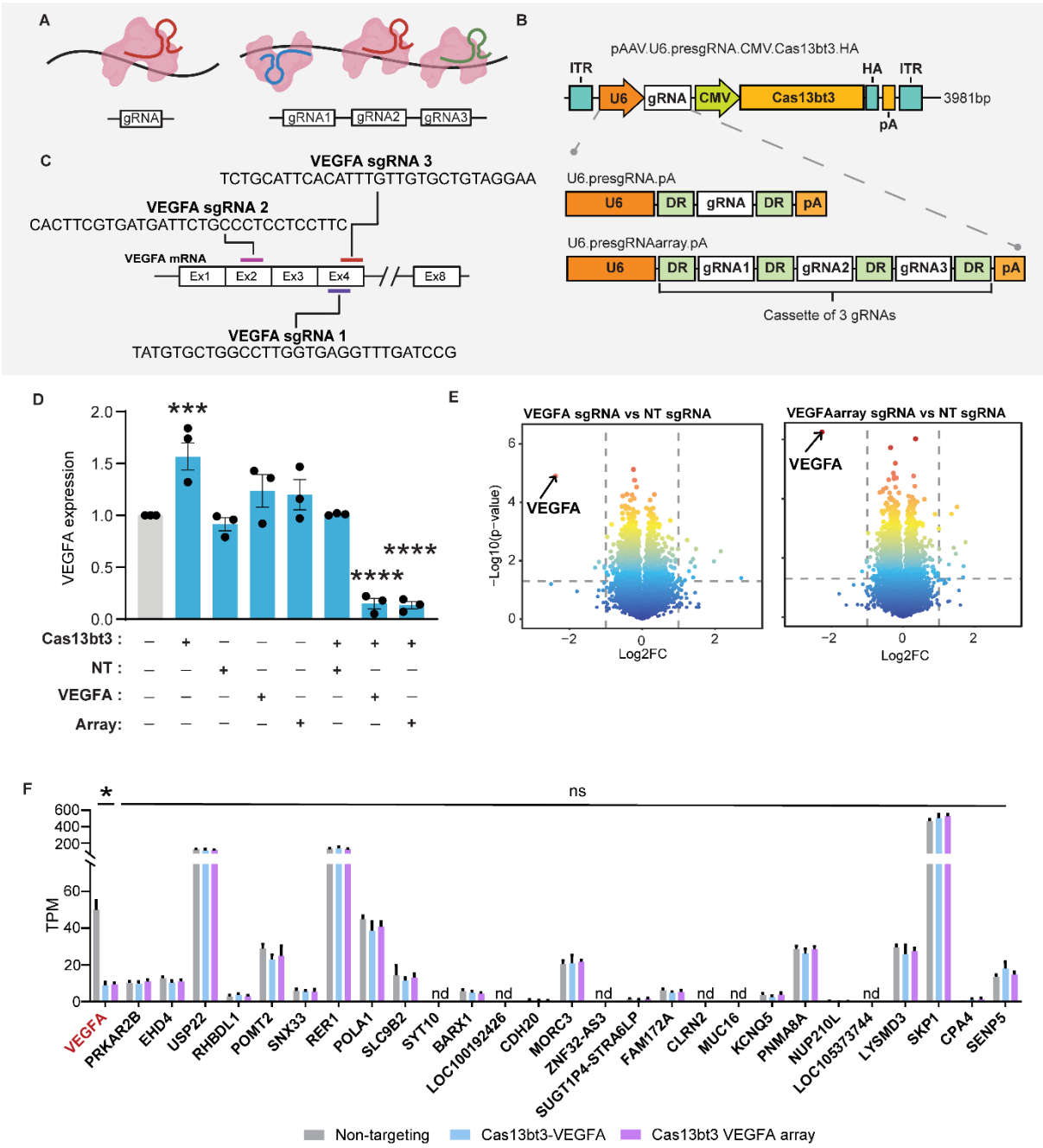

Figure 2 Guide-dependent and guide-independent off-targets from Cas13bt3-mediated VEGFA knockdown. **(A)** Schematic of single and multiplex targeting with Cas13bt3 and **(B)** U6-sgRNA domain in single sgRNA and multiple sgRNA vectors. **(C)** Guide RNA targeting regions in *VEGFA* mRNA. **(D)** *VEGFA* mRNA knockdown from Cas13bt3, non-targeting and targeting sgRNAs. **(E)** Volcano plots showing differentially expressed genes between Cas13bt3 with non-targeting and **(F)** TPM plots for VEGFA and candidate off-target genes. Target gene VEGFA is highlighted in red. Data presented as mean ± SEM. Statistical analysis

232 was conducted by one-way ANOVA and Tukey's multiple comparison test (**C**) and Welch's t-
233 test. ns: not significant, *P≤0.05, ***P≤0.0001, ****P≤0.00001.
234

235

236 **Retinal organoids can be efficiently transduced by AAV2.7m8 for expression of Cas13bt3.**

237 Human organoids are excellent models for gaining clinically relevant information on new
238 therapeutic agents, as they are derived from human pluripotent stem cells (PSCs) and reproduce
239 morphological, functional and transcriptomic features *in vitro*[23]. Recently, hESC-derived
240 retinal organoids have been used to investigate eye development and model inherited retinal
241 diseases as well as the testing of novel gene therapies[24, 25]. While CRISPR-Cas9 has entered
242 the clinic, Cas13-based therapies largely remain at the preclinical stage, and demonstrating
243 utility of Cas13 in retinal organoids will be a major advance for ocular gene therapy.

244 Here we utilised our well-established 2D/3D differentiation protocol to generate hESC-
245 derived retinal organoid containing all the major cell types in the retina[26]. First, to ensure
246 maximum expression of the Cas13 nuclease in the retinal cells, we subjected the Cas13bt3
247 protein sequence to codon optimisation to obtain two other variants of Cas13bt3 ($Cas13bt3_{COP1}$
248 and $Cas13bt3_{COP2}$) (**Figure S5A**). We compared the expression levels of the original Cas13bt3
249 with $Cas13bt3_{COP1}$ and $Cas13bt3_{COP2}$ by transfection in HEK293FT and ARPE19 cells and
250 found both variants to exhibit increased expression and knockdown efficiency (**Figure S5B, C**
251 **and D**). Among them, $Cas13bt3_{COP1}$ showed the highest expression and was used for
252 subsequent investigation. To elucidate the activity of Cas13bt3 and efficacy for AAV gene
253 therapy RNA editing in *bona fide* human retinal cells we transduced 19 weeks old organoids
254 with AAV2.7m8.U6.NTsgRNA.Cas13bt3 and AAV2.7m8.U6.VEGFAsgRNA.Cas13bt3 viral
255 vectors. Retinal organoids were then harvested for single cell RNA sequencing (scRNA-Seq)

256 6 weeks after treatment (~25 weeks) for (**Figure 3A**). First, we confirmed that the major retinal
257 cell types were clustered similarly across experimental conditions (S1: Untreated; S2:
258 AAV2.7m8.U6.VEGFAsgRNA.Cas13bt3; and S3: AAV2.7m8.U6.NTsgRNA.Cas13bt3)
259 (**Figure 3B**, n = 3 pooled organoids per condition). We used our recently described retinal atlas
260 dataset to determine fidelity of retinal organoids and identified expression of the different
261 retinal cell markers[27], confirming exclusive cell-specific expression of the markers (**Figure 3C**
262 **and S6, S7**).

263 Next, to examine Cas13bt3 expression in the retinal organoids, we evaluated read
264 numbers and classified cells containing more than 10 reads of Cas13bt3 to be positive for viral
265 infection. Using this threshold, we determined an average transduction efficiency of 18.78%
266 (1403 out of 7467 cells) for the VEGFA sgRNA group and 25.95% (2260 out of 8706 cells)
267 for the NT sgRNA group. Next, we analysed transduction and presence of Cas13bt3 in specific
268 cell types. While all cell types showed noticeable levels of Cas13bt3, RPE cells, in particular,
269 showed high levels of expression with up to 50% of cells containing Cas13bt3 in the VEGFA
270 sgRNA (S2) treatment group. Interestingly, in the NT sgRNA group, only ~15% of RPE cells
271 expressed Cas13bt3, which could owe to varying culture conditions. Bipolar cells showed the
272 least expression of Cas13bt3 (≤10%), while all other cell types showed moderate expression
273 (≤25%) (**Figure 3D**). Overall, our results indicated AAV2.7m8 as a useful delivery vector for
274 cells across retinal cell types.

275 To investigate the impact of the NT sgRNA in retinal cells, we first compared DEGs
276 between cells positive and negative for Cas13bt3 in the retinal organoid that received the
277 AAV2.7m8.U6.NTsgRNA.Cas13bt3. Here, we observed a significant number DEGs across all
278 cell types, and in similar trend to the HEK293FT cells where most DEGs were upregulated
279 genes (**Figure 3E**). Albeit at a lower extent the same pattern was observed in the retinal

280 organoid transduced with AAV2.7m8.U6.VEGFAsgRNA.Cas13bt3 (**Figure 3F**), suggesting
281 that the NT sgRNA exhibited greater impact on the transcriptome. To determine the specific
282 cell types that were more sensitive to Cas13bt3 expression, we identified unique DEGs from
283 each cell type (to remove common effects from AAV delivery and culturing conditions) across
284 the retinal cells and found macroglial and bipolar cells to exhibit the highest DEGs, which was
285 especially higher in the NT sgRNA group (Macroglial - NT: 5571 vs VEGFA: 2928, Bipolar
286 – NT: 3725 vs VEGFA: 1633) (**Figure 3G**).

287 To understand this effect from the NT sgRNA, we further identified DEGs unique to
288 the NT sgRNA and VEGFA sgRNA group and performed GO analysis to identify responses
289 exclusive to the delivered sgRNA. However, ubiquitin protein-like (UBL) associations (e.g.,
290 "*UBL ligase binding*", "*UBL transferase activity*") were top hits for both groups across
291 macroglial, bipolar, amacrine and RPE cells (**Figure 3H and Extended data 2**). Ubiquitin
292 processes are often activated in response to immune stress to facilitate the clearing of proteins
293 inside cells [28], and our results suggest the delivery of Cas13bt3 with an activating sgRNA (non-
294 targeting or targeting) to significantly elevate the immune response in retinal cells. This stress
295 response is likely higher with the NT sgRNA group due to unspecific RNA binding, causing
296 the increased transcriptomic impact. The strong stress response from all cells to Cas13bt3
297 delivery is also likely to have made sgRNA-specific responses challenging to distinguish.
298

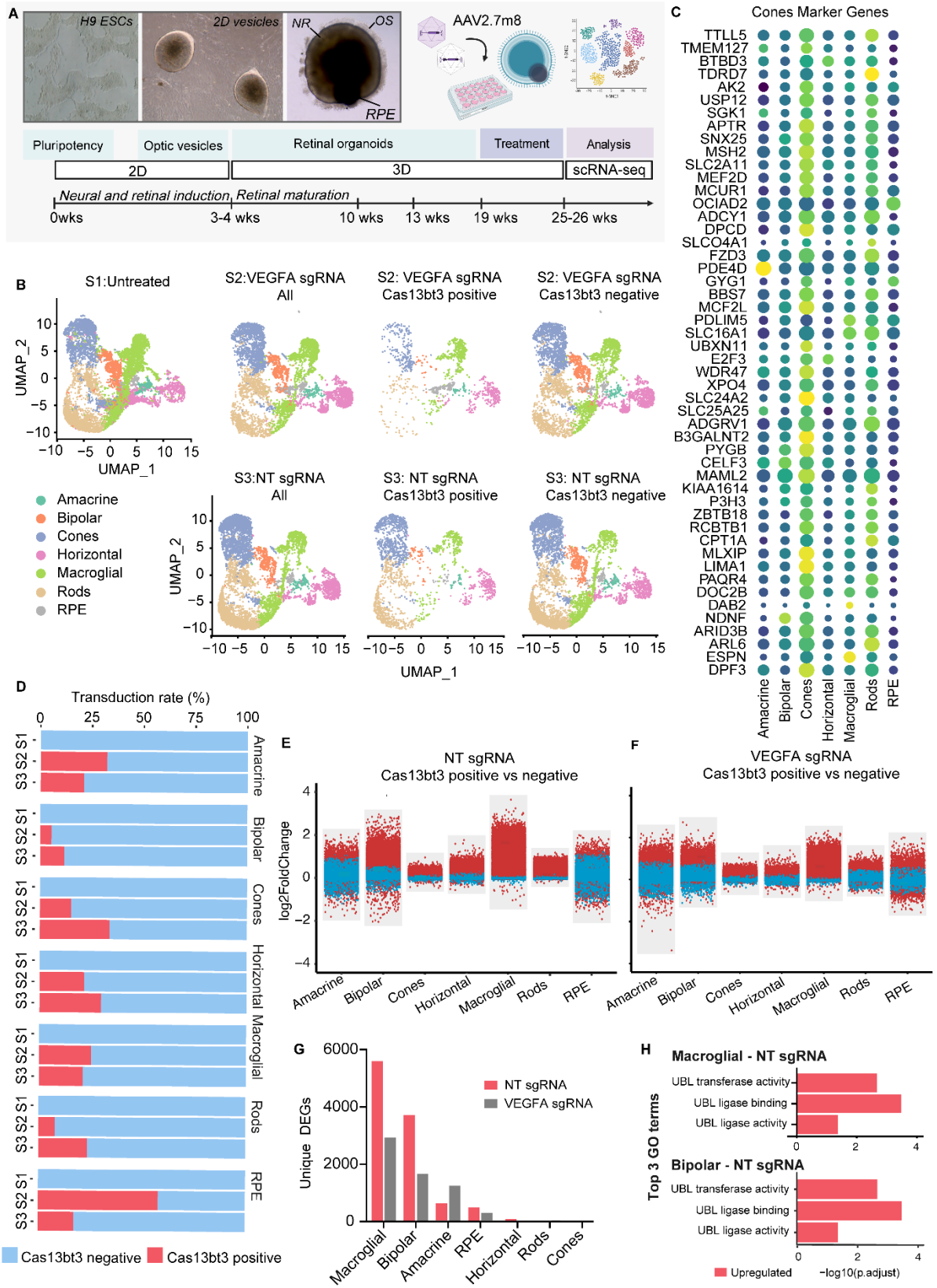
A
H9 ESCs
2D vesicles
NR
OS
RPE
AAV2.7m8
Pluripotency
Optic vesicles
Retinal organoids
Treatment
Analysis
2D
3D
scRNA-seq
Neural and retinal induction
Retinal maturation
0wks
3-4 wks
10 wks
13 wks
19 wks
25-26 wks
B
S1:Untreated
S2:VEGFA sgRNA All
S2: VEGFA sgRNA Cas13bt3 positive
S2: VEGFA sgRNA Cas13bt3 negative
S3:NT sgRNA All
S3: NT sgRNA Cas13bt3 positive
S3: NT sgRNA Cas13bt3 negative
UMAP_1
UMAP_2
Amacrine
Bipolar
Cones
Horizontal
Macroglial
Rods
RPE
C
Cones Marker Genes
TTLL5
TMEM127
BTBD3
TDRD7
AK2
USP12
SGK1
APTR
SNX25
MSH2
SLC2A11
MEF2D
MCUR1
OCIAD2
ADCY1
DPCD
SLCO4A1
FZD3
PDE4D
GYG1
BBS7
MCF2L
PDLIM5
SLC16A1
UBXN11
E2F3
WDR47
XPO4
SLC24A2
SLC25A25
ADGRV1
B3GALNT2
PYGB
CELF3
MAML2
KIAA1614
P3H3
ZBTB18
RCBTB1
CPT1A
MLXIP
LIMA1
PAQR4
DOC2B
DAB2
NDNF
ARID3B
ARL6
ESPN
DPF3
D
Transduction rate (%)
S3 S2 S1
Cas13bt3 negative
Cas13bt3 positive
E
NT sgRNA
Cas13bt3 positive vs negative
log2FoldChange
F
VEGFA sgRNA
Cas13bt3 positive vs negative
G
Unique DEGs
NT sgRNA
VEGFA sgRNA
H
Macroglial - NT sgRNA
UBL transferase activity
UBL ligase binding
UBL ligase activity
Bipolar - NT sgRNA
Top 3 GO terms
Upregulated
-log10(p.adjust)

299

300 **Figure 3. Cas13bt3 treatment and single-cell RNA sequencing of 3D retinal organoids.**
301 **(A)** Schematic of 3D retinal organoid scRNA-seq experimental procedure. **(B)** UMAP plots
302 showing retinal cell type clusters for the untreated, NT sgRNA and VEGFA sgRNA treatment
303 groups. **(C)** Expression of cell-type specific markers in cone cells. **(D)** Infection rate of retinal
304 organoids by cell type and treatment group. **(E)** Multi-volcano plots showing differentially
305 expressed genes (DEGs) between Cas13bt3 positive and negative cells from the NT sgRNA
306 and **(F)** VEGFA sgRNA treatment groups. **(G)** Number of unique DEGs across retinal cell
307 types. **(H)** GO molecular function terms related to unique DEGs from Cas13bt3-NT sgRNA
308 treatment for macroglial and bipolar cells. UBL = Ubiquitin-like protein.
309

310

311 **Cas13bt3 significantly knockdown *VEGFA* mRNA in retinal organoids.**

312 Next, we examined Cas13bt3 targeting efficiency and effect on *VEGFA* expression across the
313 retinal cell types. First, we determined *VEGFA* expression in control untreated organoids.
314 *VEGFA* mRNA is present across all retinal organoids cell types. Expression of VEGFA varied
315 significantly between retinal cell types with macroglial, rod, cone photoreceptors, and bipolar
316 cells expressing significantly less *VEGFA* than RPE cells (**Figure S8A, B**).

317 Furthermore, *VEGFA* expression was also detected in all treated organoids, albeit at
318 different levels (**Figure S8C-E**). DEGs were detected in all cell types between retinal
319 organoids transduced with Cas13bt3-VEGFA sgRNA and Cas13bt3-NT sgRNA. However, a
320 significant downregulation of *VEGFA* was only detected in RPE cells (**Figure S9**). While
321 Cas13bt3 positive cells have been identified, the abundance of Cas13bt3 reads within cells may
322 still vary (**Figure 4A**) and affect determination of targeting efficiency. We hypothesised that
323 increased intracellular Cas13bt3 transcripts allows for higher targeting efficiency and thereby
324 increased silencing of *VEGFA* mRNA (**Figure 4B**). We first examined the number of Cas13bt3
325 reads in cells that received AAV2.7m8.U6.NTsgRNA.Cas13bt3 and
326 AAV2.7m8.U6.VEGFAsgRNA.Cas13bt3 treatments (**Figure 4C and S10**). To accurately
327 determine Cas13bt3 effect and to understand abundance of the targeting complex within each

328 cell we examined AAV2.7m8.U6.VEGFAsgRNA.Cas13bt3 treated cells. Here, we found RPE
329 and macroglial cells expressed high levels of Cas13bt3 expression while most cones, rods and
330 horizontal and bipolar cells only showed low levels of Cas13bt3 expression (**Figure 4C**). We
331 selected a threshold to classify high (≥ 50 reads) and low (<50 reads) expression of Cas13bt3
332 that enables evaluation of targeting efficiency. Next, we quantified *VEGFA* mRNA expression
333 in cells expressing high and low levels of Cas13bt3. To this end, we pooled cells within the
334 high and low Cas13bt3 thresholds and compared average *VEGFA* expression against Cas13bt3
335 negative cells to determine if loss of *VEGFA* is from is dependent on high levels of Cas13bt3.
336 Significant decrease of *VEGFA* in high Cas13bt3-expressing cells compared to low Cas13bt3-
337 expressing cells would indicate *VEGFA* silencing from increased targeting activity, while
338 significant reduction compared to negative cells would indicate *VEGFA* loss from viral
339 delivery. Here, we observed that RPE cells were the only cells to show significant reduction of
340 *VEGFA* expression in the high Cas13bt3 when compared to low Cas13bt3 cells ($P < 0.05$)
341 (**Figure 4D**, red square). Viral delivery appeared to upregulate *VEGFA* expression in
342 macroglial cells with both low and high Cas13bt3-expressing cells exhibiting significant
343 increase in VEGFA expression (**Figure 4D**). Interestingly, the increase of *VEGFA* was not
344 significant between low and high Cas13bt3 expressing macroglial cells, suggesting a
345 considerable loss of *VEGFA* (**Figure 4D**). We therefore further investigated retinal cells that
346 showed moderate transduction (~25%) of Cas13bt3-VEGFA sgRNA (i.e. amacrine, horizontal
347 and macroglial) and compared *VEGFA* expression to cells that received Cas13bt3-NTsgRNA.
348 Promisingly, we observed near significant downregulation of *VEGFA* in amacrine and
349 horizontal cells ($P = 0.075$ and $P = 0.051$ respectively), suggesting higher transduction rates
350 may lead to significant downregulation in the other cells as well (**Figure S11**). We then studied
351 DEGs in the RPE cells to determine if the off-target genes previously identified were affected

352 from the significant Cas13bt3-mediated *VEGFA* silencing. Importantly, none of the off-target
353 genes we previously identified were significantly affected (**Figure 4E and S12**). Finally, GO
354 analysis revealed that "*PDGF receptor binding*" was among the top five downregulated
355 processes (**Figure 4F and Extended data 3**), akin to our observations in HEK293FT cells.

356 While we only observed significant *VEGFA* mRNA knockdown in RPE cells, whether
357 this is a result of higher transduction or RPE cells carry cell-specific factors that are conducive
358 for Cas13 activity needs further investigation. Regardless, with RPE cells being major
359 contributors of *VEGFA* expression, our results show that Cas13bt3 can be a potent tool against
360 diseases such as DR and nAMD.

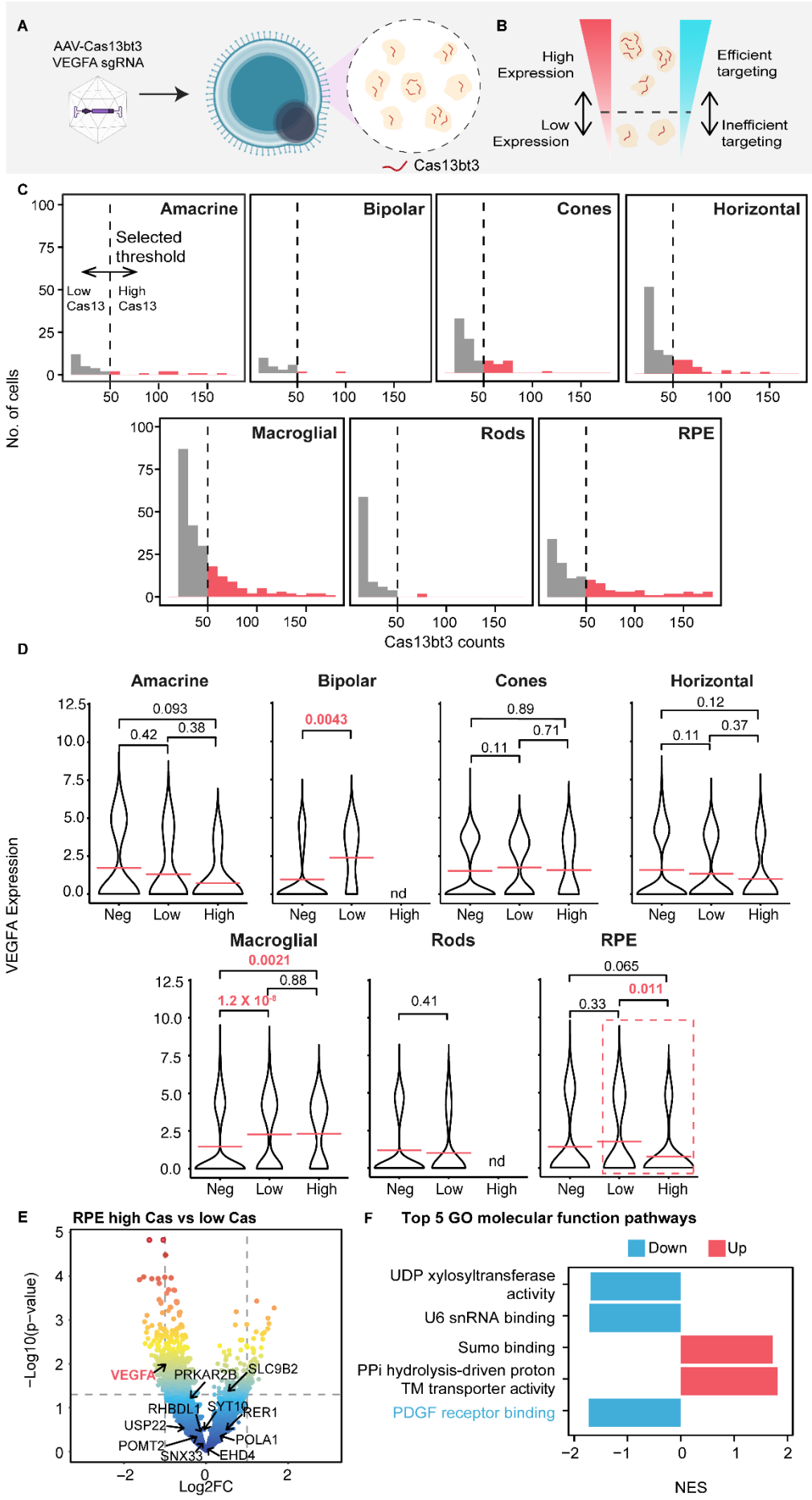
A
AAV-Cas13bt3
VEGFA sgRNA
Cas13bt3
B
High Expression
Low Expression
Efficient targeting
Inefficient targeting
C
Amacrine
Bipolar
Cones
Horizontal
Macroglial
Rods
RPE
Selected threshold
Low Cas13
High Cas13
No. of cells
Cas13bt3 counts
D
VEGFA Expression
Neg
Low
High
nd
0.093
0.42
0.38
0.0043
0.89
0.71
0.11
0.12
0.37
0.0021
1.2 X 10-8
0.88
0.41
0.065
0.011
0.33
E
RPE high Cas vs low Cas
−Log10(p−value)
Log2FC
VEGFA
PRKAR2B
SLC9B2
RHBDL1
SYT10
RER1
USP22
POLA1
POMT2
SNX33
EHD4
F
Top 5 GO molecular function pathways
Down
Up
UDP xylosyltransferase activity
U6 snRNA binding
Sumo binding
PPi hydrolysis-driven proton TM transporter activity
PDGF receptor binding
NES

361

362 ***Figure 4. VEGFA knockdown efficiency in human retinal organoids.*** **(A)** Schematic of
363 variable Cas13bt3 expression in retinal organoid cells and **(B)** relationship between CRISPR-
364 Cas13bt3 expression and targeting efficiency. **(C)** Histograms showing level of Cas13bt3
365 expression by number of reads across retinal cell types in the VEGFA sgRNA group. **(D)** Violin
366 plots of *VEGFA* expression against level of Cas13bt3 expression across retinal cell types
367 compared to Cas13bt3 negative cells. Red box indicates cells of interest for high VEGFA
368 targeting activity. **(E)** Volcano plot of DEGs between RPE cells with high and low Cas13bt3
369 expression. Significant knockdown of *VEGFA* is highlighted in red. **(F)** Top five significant
370 GO molecular function terms between RPE cells expressing low and high Cas13bt3. Statistical
371 analyses were conducted using Student's t-test **(E)**. PPi: Pyrophosphatase. TM:
372 Transmembrane.
373

374

375 **VEGFA knockdown impedes disease progression in humanised mouse model of**
376 **proliferative diabetic retinopathy.**

377 Lastly, we sought to investigate if *VEGFA* knockdown can control neovascularisation *in vivo*
378 in humanised models of DR. This offers a potential new tool against eye diseases causing
379 neovascularisation. To this end, we utilised the trVEGF029 (Kimba) mouse, a humanised
380 transgenic mouse model where the neuroretina overexpresses h*VEGFA* leading to
381 neovascularisation like human proliferative DR[29]. To ensure that optimal transduction of the
382 retina is being achieved, we delivered a mCherry reporter gene under the control of CMV
383 promoter using the AAV2.7m8 serotype, known to have excellent transduction of the retina,
384 when delivered intravitreally into C57BL/6 mice (**Figure S13A and B**).
385 Immunohistochemistry analysis of AAV2.7m8.CMV.mCherry treated retinal flatmounts
386 showed high levels of fluorescence through all retinal layers (RGCs, bipolar and photoreceptor
387 cells) 4 weeks following injections, confirming quick onset and deep penetration of the retina
388 from intravitreal delivery (**Figure S13C, n = 6 eyes from 3 animals**).

389 Next we treated Kimba mice with AAV2.7m8 viruses driving our codon optimised
390 Cas13bt3 carrying NT sgRNA (AAV2.7m8.U6.NTsgRNA.Cas13bt3) or VEGFA sgRNA

391 (AAV2.7m8.U6.VEGFAsgRNA.Cas13bt3). Due to severe disease progression in homozygous
392 Kimba (*VEGFA*$^{+/+}$), we opted for the heterozygous (*VEGFA*$^{+/-}$) breed. Six-week-old Kimba
393 mice received bilateral, intravitreal injections of AAV2.7m8.U6.NTsgRNA.Cas13bt3 or
394 AAV2.7m8.U6.VEGFAsgRNA.Cas13bt3. Eight weeks following treatment eyes were
395 analysed for *VEGFA* mRNA expression, neovascular growth, and retinal degeneration (**Figure**
396 **5A**). Similar to the control mCherry treatments, high transduction of photoreceptor cells was
397 observed as demonstrated by co-localisation of mCherry and HA-tag (Cas13bt3) with
398 Rhodopsin positive cells in the ONL (**Figure 5B, C**). In addition qPCR analysis showed high
399 expression of Cas13bt3 in Kimba retinas injected with AAV.2.7m8.U6.NTsgRNA.Cas13bt3
400 and AAV2.7m8.U6.VEGFAsgRNA.Cas13bt3 (**Figure 5D,** n = 3-12 retinas). This
401 corresponded with ~50% reduction ($P < 0.001$) of human VEGFA (*hVEGFA)* mRNA (**Figure**
402 **5E**), but not mouse VEGFA (mVEGFA) (**Figure 5F**) in the
403 AAV2.7m8.U6.VEGFAsgRNA.Cas13bt3 group, while no reduction was observed with
404 AAV2.7m8.U6.NTsgRNA.Cas13bt3 or no treatment (**Figure 5E, F,** n = 3-12 retinas). These
405 results confirmed specific knockdown of *hVEGFA* from Cas13bt3, despite high
406 complementarity of *VEGFA* sequences (29 out of 30 nucleotides) in the targeting region
407 (**Figure 5G**). RNA sequencing further confirmed that mouse VEGFA expression and predicted
408 off-target genes were not significantly altered, indicating safety of Cas13bt3-mediated RNA
409 silencing (**Figure S13**).

410 To confirm if *VEGFA* mRNA knockdown influenced disease progression, we analysed
411 fundus fluorescein angiography (FFA) images from Kimba eyes for vessel leakage and
412 quantified vessel density and number of branch points, which are signs indicative for the
413 neovascular process. We used fluorescein to label vessels of the
414 AAV2.7m8.U6.VEGFAsgRNA.Cas13bt3, AAV2.7m8.U6.NTsgRNA.Cas13bt3 and untreated

415 eyes. We observed large spots of vessel leakage, indicating neovascularisation had progressed
416 in both untreated and NT treated eyes (**Figure 5H,** green expression and white arrows).
417 However, in the AAV2.7m8.U6.VEGFAsgRNA.Cas13bt3 group, no leakage was observed
418 (**Figure 5H,** VEGFA targeting). Immunohistochemistry against laminin was used to image
419 through the retinal vascular layers (superficial, intermediate and deep vascular plexuses)
420 (**Figure S16A and B**). Blood vessels appeared diminished in the intermediate and deep
421 vascular layers for the VEGFA sgRNA group. In the NT sgRNA group, the neovascular
422 process could be observed through leaky vessel structure in the same layers (**Figure S16C,** n
423 = 4 retinas). The AAV2.7m8.U6.VEGFAsgRNA.Cas13bt3 treated eyes also showed
424 significantly lower vessel density and branch points compared to baseline at 6 weeks post-
425 treatment, unlike the untreated and the AAV27m8.U6.NTsgRNA.Cas13bt3 eyes (**Figure 5I**
426 **and J,** n = 4-13 retinas, $P<0.05$). Next, to determine whether *VEGFA* knockdown leads to
427 rescue of overall retinal structure. we performed optical coherence tomography (OCT) to
428 analyse total retinal thickness (TRT) before and after treatments. We observed no significant
429 changes between the untreated and treated groups, and a general decline in TRT across all
430 animals (**Figure S17**). We postulate that the overexpression of *hVEGFA* promotes rapid retinal
431 degeneration that could not be controlled or reversed through *VEGFA* silencing.

432 Overall, our findings showed Cas13bt3-mediated RNA silencing to significantly reduce
433 *VEGFA* mRNA expression, specifically target *hVEGFA* and control hallmark signs of
434 neovascularisation in a humanised mouse model, promising a useful alternative to current anti-
435 VEGF drugs.

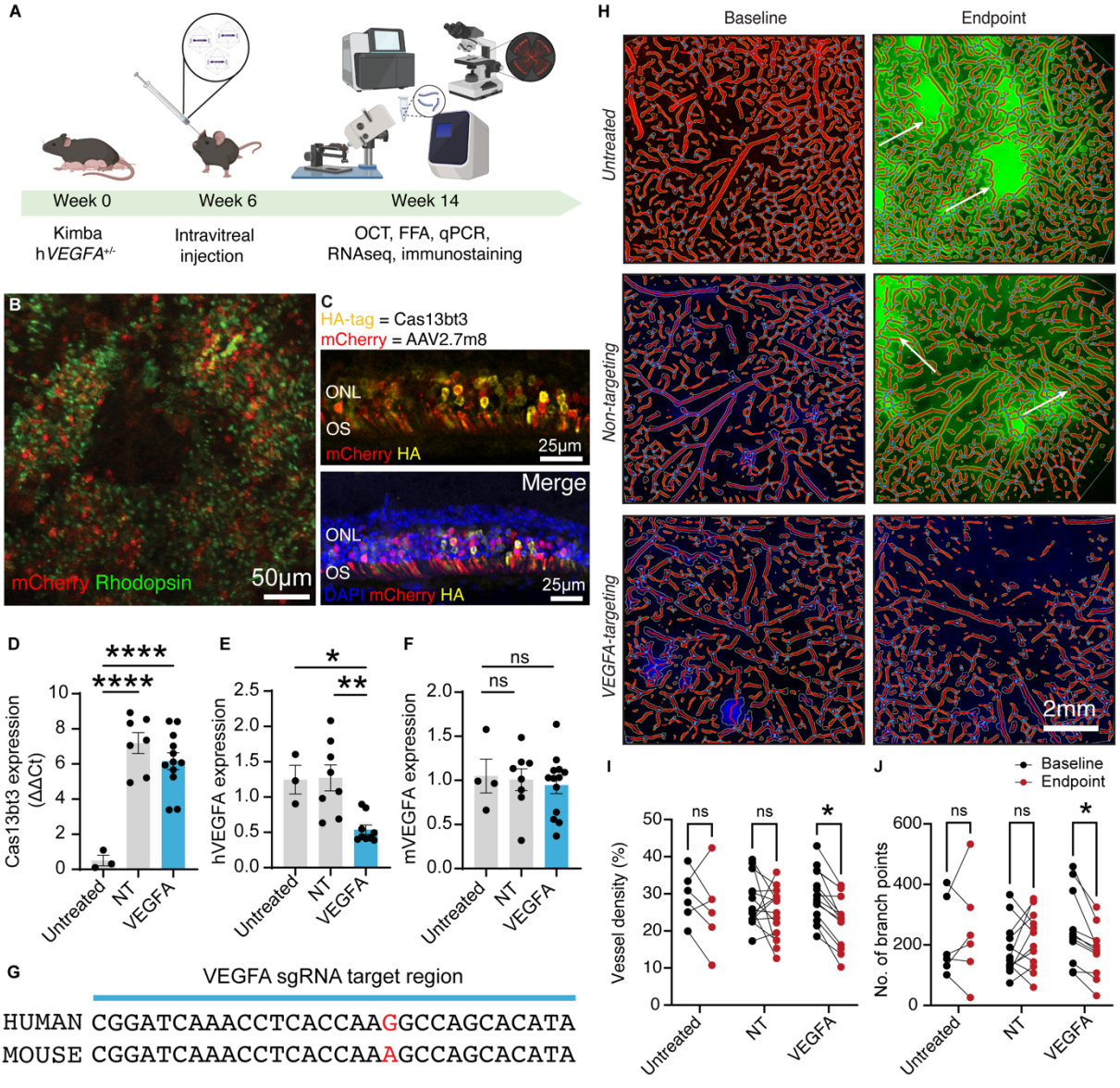

Figure 5. In vivo VEGFA mRNA knockdown in humanised Kimba mice. **(A)** Schematic of experimental procedure for intravitreal treatment of Kimba mice. **(B and C)** Immunohistochemistry of retinal flatmount and cryosection showing transduction of AAV2.7m8 and expression of Cas13bt3 (Magnification: 20X and 40X, respectively). **(D)** Expression of Cas13bt3 from Kimba mice retinas. **(E)** Expression of mouse and human *VEGFA* mRNA in Kimba retinas. **(F)** *VEGFA* mRNA targeting regions in human and mouse transcriptome. **(G)** Plot of vessel density and number of branch points from untreated and treated Kimba eyes at baseline (6 weeks) and endpoint (14 weeks) analysed from *in vivo* central fluorescein fundus angiography (FFA). **(H)** Central fluorescein fundus angiography (FFA) images obtained from Kimba mice at baseline (6 weeks) and endpoint (14 weeks) after AngioTool analysis and quantification. Images were edited using Adobe Photoshop to remove central retinal arteries and veins. Green spots and white arrows indicate leakage from blood vessels. Data presented as mean ± SEM. Statistical analysis was conducted by one-way

450 ANOVA (**D and E**) with Tukey's multiple comparison test and Multiple paired t-tests (**G**).
451 *P≤0.05, **P ≤0.001, ****P≤0.00001.
452

453

454 **DISCUSSION**

455 Our comprehensive *in vitro*, *ex vivo* and *in vivo* characterisation of Cas13bt3 activity and
456 performance in the retina provides novel insights for therapeutic use of the enzyme. Cas13bt3
457 was first described only two years ago but has garnered significant attention for its compact
458 size and reported specificity[11]. Structural characterisation and activation mechanisms have
459 recently been described spearing immense interest in the molecule for therapeutic
460 development[16, 30]. Due to ongoing controversy over the exact specificity of Cas13 nucleases[10],
461 we aimed to characterise Cas13bt3 efficiency and specificity in mouse and human cells. We
462 chose to target the *VEGFA* transcripts, as this growth factor is essential for both physiological
463 and pathological angiogenesis. In the retina, physiological functions include its role as a
464 survival factor for retinal ganglion cells[31], photoreceptors, Müller cells[32], and RPE[33]. In
465 disease, overexpression of VEGFA leads to neovascularisation and vision loss. Therefore,
466 clinical applicability of VEGFA downregulation in specific cell types of the retina is of great
467 importance.

468 Previous studies have demonstrated transcript knockdown using CasRx proteins[11, 12].
469 Notably, CasRx-mediated *VEGFA* mRNA knockdown has also been shown to reduce choroidal
470 neovascularisation after silencing VEGFA in RPE cells *in vivo* in laser-induced choroidal
471 neovascularisation model[4]. Our results confirmed that Cas13bt3 mediates significant
472 knockdown of *VEGFA* in human cell lines, hESC-derived retinal cells, and the mouse retina.
473 We further investigated the transcriptomic impact of expressing active Cas13bt3 in the cells
474 and found that initiating Cas13bt3's target search process with a non-targeting sgRNA can lead

475 to significant RNA binding, upregulating the expression of several genes. A targeting sgRNA,
476 such as with VEGFA, appears to narrow the target-search process and thereby reduce
477 transcriptomic impact.

478 *In vitro*, and specifically in HEK293FT cells, several studies have shown Cas13
479 nucleases to be highly precise[10]. Most of these studies, however, compared differentially
480 expressed genes to a NT control, not accounting for transcriptomic perturbations from a Cas13-
481 NT sgRNA complex. A recent study showed high collateral activity from CasRx when
482 compared to an empty vector[34]. Here, we compared targeting Cas13bt3 to vector controls
483 showing minimal, but positive collateral activity. More importantly, we show that Cas13 with
484 a NT sgRNA has significant transcriptomic impact resulting in high levels of DEGs. This
485 demonstrates that NT sgRNAs are not appropriate controls for determining specificity of Cas13
486 nucleases raising awareness against their use.

487 We also show that multiple sgRNAs can be incorporated within a single AAV vector
488 with Cas13bt3 driven by a strong ubiquitous promoter (CMV) for targeted knockdown of
489 *VEGFA* mRNA. Even though this appears to be an attractive approach to enhance transcript
490 knockdown our study established that multiple sgRNAs failed to improve transcript
491 degradation. The rate of mRNA knockdown was comparable to single sgRNA treatments.
492 Previously, we similarly observed with multiplexed RNA editing with CasRx carrying three
493 *VEGFA*-targeting sgRNAs, the multiple sgRNA system unexpectedly led to decreased
494 knockdown efficiency[19], raising the suspicion that substrate competition or inadequate Cas13
495 activation plays an inhibitory role in RNA targeting efficiency. Interestingly, the comparable
496 levels of DEGs in both single and multiple sgRNA vectors suggest that Cas13bt3 activation is
497 not drastically elevated with the presence of additional sgRNAs. While we did not investigate
498 the delivery of sgRNAs targeting multiple genes, our results show multiple sgRNAs do not

499 increase overall collateral activity, which might prove useful when several genes must be
500 targeted simultaneously to control disease progression. This approach could potentially be
501 applied even to ocular neovascularisation by simultaneously targeting the *VEGFA* and *PDGF*
502 genes for enhanced treatment[35].

503 Furthermore, we investigated for the first time AAV-mediated Cas13 RNA expression
504 and editing in retinal organoids at single cell resolution. While several studies have
505 demonstrated *VEGFA* silencing for control of neovascularisation, previous studies have
506 focused on specific cell types that are believed to be major contributors to *VEGFA* expression,
507 like RPE and Müller cells[4, 36]. While this proves useful to demonstrate proof-of-concept, it does
508 not provide a comprehensive understanding relevant for therapeutic development as *VEGFA*
509 silencing in one cell type may have collateral effects on other retinal cells. Retinal organoid
510 models enable the testing of therapies in an environment that mimics the human retina
511 containing lamination and major retinal cell types of the developing retina. Here we sought to
512 understand retina-wide effect following delivery of Cas13bt3 as well as targeted silencing of
513 *VEGFA*. Our findings not only support the use of Cas13bt3 for ocular gene therapy, but also
514 brings to light several considerations for its use. First, we showed transduction across all retinal
515 cell types studied with the clinically relevant AAV2.7m8 vector (NCT04418427) confirming
516 its effectiveness as a vector for retinal transduction and supporting its clinical utility[37,38].
517 Among the retinal cell types studied, bipolar cells showed the least transduction by AAV2.7m8,
518 while RPE cells seemed more susceptible. It is likely that these differences are due to cell-
519 specific transduction susceptibility, as RPE cells are easily transduced with a variety of AAV
520 capsids[39]. It should also be noted that overall transduction was determined using an arbitrary
521 cut-off (Cas13bt3 read counts $\geq$ 10) based on our previous experience with the retinal
522 organoids[26]. NT sgRNA activity following gene therapy led to numerous DEGs when

523 compared to VEGFA targeted sgRNA. This emphasises the need for a well-designed targeting
524 sgRNA for reduced collateral activity. Retinal organoids showed significantly more DEGs than
525 HEK293FT cells, which is expected partly due to cellular response to virus delivery. Still,
526 notwithstanding response to AAV, the higher DEG levels also indicate that retinal cells are
527 more sensitive to Cas13, demonstrating the importance of studying nuclease activity and
528 efficiency in physiological relevant models, an important consideration for Cas-mediated gene
529 therapies. As preclinical studies with Cas13 nucleases are commonly performed in HEK293FT
530 cells, its specificity has often been exaggerated in the literature. Our results strongly suggest
531 that Cas13 specificity must be evaluated in relation to untreated or empty vector controls in
532 organ-specific cells to accurately determine safety. On the front of therapeutic potential, we
533 could only confirm significant targeted *VEGFA* mRNA knockdown in RPE cells, which is
534 likely due to strong expression of Cas13bt3 in these cells. Lower copies of Cas13bt3 in the
535 other cells may have resulted in the lack of significant *VEGFA* knockdown, and further studies
536 are required to understand the levels of Cas13 expression necessary in other retinal cells for
537 effective activity. Testing of cell type specific promoters could be beneficial as CMV promoter
538 is known for its susceptibility to silencing in certain cell types, for example stage specific PSC-
539 derived photoreceptor cells (REF). Importantly, with RPE cells being the primary producers of
540 *VEGFA* in the retina, the significant downregulation of *VEGFA* mRNA in RPE strongly
541 suggests the benefits of Cas13bt3 gene therapy as a potential anti-VEGF tool for neovascular
542 eye disease.

543 Lastly, we tested the anti-VEGF potential of Cas13bt3 in the retina of a humanised
544 mouse model of diabetic retinopathy, the Kimba mouse. We opted to examine anti-VEGF
545 potential of Cas13bt3 in Kimba mice as it shows chronic disease and all major signs of
546 proliferative retinopathy [29]. Importantly, as Kimba mice expresses human *VEGFA*, the same

547 vectors tested in retinal organoids could also be used *in vivo*. Others have shown the control of
548 ocular neovascularisation using mouse models of laser-induced injury[4], streptozotocin (STZ)-
549 induced diabetes[40], or oxygen-induced retinopathy (OIR)[41]. However, these models have some
550 drawbacks. The laser-induced choroidal neovascularisation model often used in anti-VEGF
551 preclinical studies does not accurate model the chronic retinal degeneration observed in DR
552 and nAMD patients and presents *VEGFA* overexpression only as a response to injury[42].
553 Diabetic mouse models do not recapitulate proliferative retinopathy which is often the cause
554 of severe vision impairment. Vascular pathogenesis is also delayed and varied based on
555 response to STZ[43]. OIR mouse models rapidly present proliferative retinopathy, however
556 neovascularisation regresses within a week[44].

557 Following RNA editing gene therapy in Kimba retinas, we demonstrated the specific
558 knockdown of human *VEGFA*, with no significant impact on endogenous mouse *VEGFA*. This
559 shows strong evidence for the specificity of targeted Cas13bt3 activity. Silencing of Cas13bt3
560 VEGFA also rescued vascular phenotypes showing an improvement in controlling vascular
561 growth and leakiness. The major concern with current anti-VEGF treatment is the need for
562 frequent intravitreal injections. Recent efforts to address this problem have employed gene
563 editing strategies like targeting *VEGFA* using CRISPR-Cas9 [36, 45]. However, efficacy of such
564 treatments are limited by efficient and safe delivery of vectors due to the size of Cas9[46, 47], poor
565 efficiency of compact Cas9 nucleases[48] or have reported the risk of genomic alterations from
566 long-term expression of Cas9[49]. Our results indicate that a single intravitreal injection could
567 achieve durable and potent while reversible silencing of *VEGFA*, addressing drawbacks with
568 current gene editing strategies. While RNA editing is thought to be safer than DNA-targeting
569 options, it is prudent to consider effects of long-term Cas13 expression, and Cas13 systems
570 amenable to regulation are of consideration for therapeutic development.

571 There are a few limitations to our study. First, we did not extensively study Cas13bt3
572 expression in ARPE19 cells, where we also observed potent knockdown. While HEK293FT
573 appears resistant to high levels of collateral activity, ARPE19 cells may exhibit significantly
574 higher levels of transcriptomic effects. This is supported by the high levels of DEGs we
575 observed in various cells from the retinal organoids, suggesting significant inflammatory
576 responses as well as cell-specific collateral activity. Specifically, the upregulation of UBL
577 processes across cell types regardless of VEGFA silencing, strongly indicate increased cellular
578 stress from delivery of Cas13. As RNA targeting molecules like Cas13 require persistent
579 expression for therapeutic effect, this could pose a significant safety concern. Second, while
580 vessel density and branching were noticeably reduced, we could not extensively study recovery
581 of phenotype in our mouse model due to severity of the disease. OCT readings showed
582 significant retinal degeneration at treatment timepoint, making rescue of phenotype
583 challenging to assess. Lastly, we were also unable to confirm reduction of VEGFA protein
584 from the mice retinas as not enough protein could be obtained for quantitative analysis.
585 CRISPR-Cas technology has advanced at breakneck speed in the last decade
586 revolutionising medicine and offering potential treatment opportunities to numerous previous
587 uncurable diseases. The recent FDA approval of an *ex vivo* CRISPR therapy for sickle-cell
588 disease (branded Casgevy) is evidence of this progress. However, a comprehensive
589 understanding of the CRISPR nucleases is crucial. In this study we offer novel insights into
590 Cas13 targeting mechanisms and its utility in targeting retinal and RPE cells providing
591 evidence for the potential of Cas13-based therapies for ocular disease. This study demonstrated
592 that the hypercompact Cas13bt3 can be efficiently delivered and expressed in various retinal
593 cell types effectively controlling *VEGFA* expression and neovascularisation. In-depth

594 evaluation of collateral activity in retinal cells would facilitate development of a safe and
595 effective Cas13-mediated anti-VEGF AAV gene therapy.
596

597 **MATERIALS AND METHODS**

598 **Plasmid construction**

599 The protein sequences of CasRx and Cas13bt3 were gifts from P. Hsu[50] and H. Yang[11],
600 respectively. Cas13bt3 was codon optimised using online tools from Integrated DNA
601 Technologies (IDT), GenScript and Benchling. The all-in-one AAV plasmids for shRNA,
602 CasRx and Cas13bt3 were designed as previously described[19], and synthesised by GenScript.
603 All plasmids used in this study are available from Addgene.

604

605 **Cell culture and transfections**

606 HEK293FT cells (American Type Culture Collection, ATCC) were maintained in Dulbecco's
607 Modified Eagle's Medium (DMEM; Thermo Fisher Scientific) supplemented with 10% (v/v)
608 fetal bovine serum (FBS, Bovogen Biologicals) and 1% (v/v) antibiotic-antimycotic (Thermo
609 Fisher Scientific) in a humidified 5% CO_2 incubator at 37°C. ARPE19 (ATCC) cells were
610 maintained in DMEM/F-12 (Thermo Fisher Scientific) supplemented with 10% (v/v) FBS and
611 1% (v/v) antibiotic-antimycotic.

612

613 **RT-qPCR**

614 At 48 hours after transfection, RNA was extracted from cells using the Monarch® Total RNA
615 Miniprep Kit (New England Biolabs and 200ng of RNA was converted to complementary DNA
616 (cDNA) using High-Capacity cDNA Reverse Transcription Kit (Thermo Fisher Scientific)
617 according to the manufacturers' instructions. cDNA was diluted with water at the ratio of 1:10.
618 qPCR was performed with 2uL of cDNA using the TaqMan™ Fast Advanced Master Mix
619 (Thermo Fisher Scientific) according to manufacturers' instructions with the following
620 TaqMan probes human VEGFA (Hs00900055_m1; Thermo Fisher Scientific), mouse VEGFA

621 (Mm00437306_m1; Thermo Fisher Scientific), human GAPDH (Hs02786624_g1; Thermo
622 Fisher Scientific), mouse GAPDH (Mm99999915_g1, Thermo Fisher Scientific). Mouse
623 eyeballs were enucleated and stored in 4°C in RNALater® until dissection. Retina was dissected
624 from injected animals and placed in lysis buffer and sonicated for 2 seconds prior to RNA
625 extraction and qPCR as previously described.
626
627 **Western blot**
628 At 48 hours after transfection, cells were harvested and collected in Pierce™ RIPA buffer
629 (Thermo Fisher Scientific) containing Pierce™ Phosphatase Inhibitor Mini Tablets (Thermo
630 Fisher Scientific). Cell lysate was sonicated for 5 seconds and centrifuged for 15 minutes at
631 13300rpm at 4°C. The supernatant was collected, and protein levels were quantified using the
632 Pierce™ BCA Protein Assay Kit (Thermo Fisher Scientific) as per manufacturers' instructions.
633 For Western blot, 10µg of protein mixed with NuPAGE™ LDS Sample Buffer (4X) (Thermo
634 Fisher Scientific) and loaded in NuPAGE™ 4 to 12% Mini Protein Gel (Thermo Fisher
635 Scientific) for gel electrophoresis at 150V for 30 minutes. Transfer to Amersham™ Hybond™
636 PVDF membrane (Cytiva) was performed at 30V for 1 hour. Protein blot was blocked with 5%
637 skim milk for 1 hour, followed by incubation with HA-tag (C29F4) Rabbit mAb (Cell Signaling
638 Technology®) or Anti-Actin Antibody, clone C4 (Merck) overnight at 4°C. Blots were then
639 stained with Goat anti-Mouse IgG (H+L) Cross-Adsorbed Secondary Antibody, HRP
640 (Invitrogen™) or Goat anti-Rabbit IgG (H+L) Secondary Antibody, HRP (Invitrogen™) for 2
641 hours at room temperature. Blot was incubated with Pierce™ ECL Western Blotting Substrate
642 for 1 minute before imaging using Bio-Rad ChemiDoc. All washes were performed with 1X
643 PBST for 5 minutes, repeated 3 times.

644

645 **ELISA**

646 At 48 hours after transfection, 100µL of supernatant was collected and ELISA was performed
647 using the Human VEGF DuoSet ELISA (R & D Systems) as per manufacturers' instructions.
648 Briefly, 96-well plates were incubated with Capture Antibody in ELISA Plate coating buffer
649 overnight at room temperature. Plates were then blocked with Reagent Diluent for 1 hour at
650 room temperature, and 100uL of supernatant was incubated for 2 hours at room temperature.
651 Then, Detection antibody was added and incubated for 2 hours at room temperature. After
652 incubation with Streptavidin-HRP and Substrate reagent for 20 minutes each, the provided stop
653 solution was added, and plate was read using the Tecan Spark® Micro plate reader at 450nm
654 with reference wavelength 570nm.

655

656 **Immunohistochemistry**

657 Retinal flatmounts were washed with 1X PBS containing 0.5% Triton-X-100 (PBST) and
658 permeabilised in -80°C for 15 minutes. After washing with PBST, flatmounts were incubated
659 in anti-rhodopsin antibody (1:500; Abcam) with 2% donkey serum and 2% PBST in 4°C for
660 72 hours. This was followed by incubation in Alexa Fluor 488 AffiniPure Donkey Anti-Mouse
661 IgG (H+L) (1:500; Jackson ImmunoResearch) at room temperature for 2 hours. After washing,
662 the flatmounts were stained with Anti-Laminin-2 (α-2 Chain) antibody, Rat monoclonal (1:250;
663 Merck) and incubated in 4°C for 5 nights. This was followed by incubation in Alexa Fluor®
664 647 AffiniPure Donkey Anti-Rat IgG (H+L) (1:250; Jackson ImmunoResearch) at room
665 temperature for 2 hours. Then, the retinae were washed and incubated in mCherry Monoclonal
666 Antibody (16D7), Alexa Fluor 594 (1:500; Thermo Fisher Scientific) at 4°C for 72 hours.
667 Retinal cryosections were blocked using serum-free protein block (Agilent Dako) at room

668 temperature for 1 hour, followed by incubation at 4°C overnight with primary antibody as
669 previously described. Secondary antibody incubation was performed at room temperature for
670 1 hour as previously described. Slides were stained with NucBlue™ Live ReadyProbes™
671 Reagent (Hoechst 33342; Thermo Fisher Scientific) for 10 minutes before mounting as
672 previously described and imaged on the Stellaris 5 confocal microscope.
673
674 **hESC Maintenance and Retinal Differentiation Culture**
675 hESCs were maintained on feeder-free conditions on E8 (Thermo Fisher) and Geltrex-coated
676 six-well plates. In brief, for retinal differentiation hESCs were maintained until 90%–95%
677 confluent, then FGF-free medium was added to the cultures for 2 days followed by a neural
678 induction period where RPE and retinal vesicles appeared. NRVs were excised and kept in low
679 binding 96-well plates for maturation.
680
681 **AAV transduction of retinal organoids**
682 Retinal organoids were maintained in ALT90 medium as previously described (West et al.,
683 2022) and AAV transduction was performed during the 15-19 weeks of differentiation. On the
684 day of transduction, AAV vectors were diluted in 300µL of fresh ALT90 medium at titer of
685 1x10E11 vg/organoids. The following day treated wells were supplemented with 700µL of
686 fresh ALT90 medium. Transduced organoids were incubated for 72 hours in the AAV vector-
687 containing medium. After the 72-hour incubation, the vector-containing medium was aspirated,
688 and 1mL of fresh ALT90 medium was added to each well. Transduced organoids underwent 6
689 weeks culture until harvesting for experimental procedures.
690

691 **Immunohistochemistry of retinal organoids**

692 Retinal organoids were fixed for 45 minutes in 4% paraformaldehyde and incubated overnight
693 in 20% sucrose, prior to embedding in OCT. Cryosections (14 µm thick) were collected for
694 analysis and preserved at - 20°C. Cryosections were blocked in 5% goat serum and 1% bovine
695 serum albumin in PBS for 2 hours. Primary antibodies (ARR3: 1:200, Rhodopsin: 1:1000,
696 VSX2: 1:200, CRALBP: 1:200, PROX1:1:200, and HuCHuD:1:500) were incubated overnight
697 at 4°C in blocking solution with 5% goat or donkey serum. After washing of primary antibody
698 with PBS sections were incubated with secondary antibody in blocking solution for 2 hours at
699 RT, washed and counter-stained with DAPI (Sigma-Aldrich). Alexa fluor 488 and 546
700 secondary antibodies (Thermo Fisher Scientific) were used at a 1:500 dilution.

701

702 **Intravitreal injections**

703 All animal procedures were approved by the Animal Ethics Committees of University of
704 Melbourne and conducted in accordance with The Association for Research in Vision and
705 Ophthalmology (ARVO) Statement for the Use of Animal in Ophthalmic and Vision Research.
706 Ethics approval was obtained from The Florey Institute of Neuroscience and Mental Health
707 Animal Ethics Committee (22-036-UM). The Akimba mice developed by Rakoczy *et al.* [51] and
708 the heterozygous Kimba mice ($hVEGFA^{+/-}$) were used for this study. Mice were bred in the
709 Melbourne Brain Centre animal facility (Kenneth Myer Building, Parkville, VIC, Australia),
710 and were housed in a well-ventilated environment that was kept at a constant room temperature
711 of 21°C, with a 12-hour diurnal light-dark cycle (lights on: 7am, off: 7pm; room illumination
712 < 50 lux). Mouse chow (Barastoc, Melbourne, VIC, Australia) and water were provided ad
713 libitum. 6-week-old Kimba mice were anesthetized with ketamine (80mg/kg) and xylazine
714 (10mg/kg) solution mix (Troy Laboratory, Smithfield, NSW, Australia; i.p. with 30G needle)

715 and given a drop of 0.5% proxymethacaine hydrochloride (Alcaine™, Alcon Laboratories,
716 Frenchs Forest, NSW, Australia) and 0.5% tropicamide (Mydriacyl™, Alcon Laboratories).
717 Baseline fundus fluoresceine angiography (FFA) were taken (as described below), and animals
718 intravitreally injected with 1uL of AAV2.7m8 viruses using Hamilton syringe attached to a 33-
719 gauge dental needle. Post injection, mice were subcutaneously administered 0.3mL of
720 atipamezole hydrochloride (0.25mg/mL) and allowed to recover on heating pads with food and
721 water *ad libitum*.
722
723 **Fundus fluorescein angiography and optical coherence tomography**
724 Retinal vasculature was assayed at baseline prior to intravitreal injection of AAVs and 8 weeks
725 after AAV-treatment using fundus fluorescein angiography (FFA) (Spectralis, Heidelberg
726 Engineering, Heidelberg, Germany) immediately after intraperitoneal injection of sodium
727 fluorescein (1%, 100 µL/kg, fluorescite 10%; Alcon Laboratories). Five images (central, nasal
728 superior, temporal superior, nasal inferior, and temporal inferior) were obtained for each eye
729 and analysed using AngioTool[52] for vessel density and branch points using default settings.
730 *In vivo* retinal structure was assayed with spectral domain optical coherence
731 tomography (SD-OCT) (Spectralis®, Heidelberg Engineering, Heidelberg, Germany) with
732 general anaesthesia, mydriasis and corneal hydration (Systane, Alcon Laboratories)
733 maintained. During image acquisition, retinal volumes (8.1 × 8.1 × 1.9 mm) centred on the
734 optic nerve head were acquired each consisting of 121 evenly spaced horizontal B-scans. Each
735 B-scan comprised of 768 A-scans with 3.87 µm axial depth resolution, 9.8 µm lateral
736 resolution. OCT scans were captured with an automated real-time tracking average of 6 frames,
737 at an average speed of 85,000 A-scans per second. The Heidelberg Eye Explorer 2 OCT reader
738 plugin (Heidelberg Engineering) was used for analysis. All retinal layers (retinal nerve fibre

739 layer, RNFL; ganglion cell inner plexiform layer, GCIPL; inner nuclear layer, INL; outer
740 plexiform layer, OPL; outer nuclear layer, ONL; photoreceptor segments, PR segment) as well
741 as total retinal thickness (TRT) were automatically segmented (Heidelberg Eye Explorer 2
742 software). A circular ring around the optic nerve head (Early Treatment Diabetic Retinopathy
743 Study [ETDRS] outer ring) was employed for analysis.
744
745 **Determination of candidate off-target genes**
746 Off-targets of the gRNAs were predicted using a sequence-based approach. gRNAs in length
747 of 30 bps were first aligned to the human transcriptome (Grch38 cdna from emsembl release
748 100) using blastn (megablast). Flexible options were set to capture the potential offtargets
749 which could tolerate up to 7 mismatches in this step, i.e., max_target_seqs = 10000, evalue =
750 10000, word_size = 5, perc_identity = 0.6. Secondly, the candidates were further filtered with
751 the threshold that at least 13 bp perfect match should exist in each alignment.
752
753 **Bulk RNA-seq data analysis**
754 Raw data processing was performed using FASTQC [53] to check the reads quality and
755 Trimmomatic [54] tool to further remove the bases and reads with low quality, adaptors and
756 barcodes. The clean reads were aligned to the reference human genome (version GRCh38),
757 utilizing STAR v2.7 [55] as the aligner. For RNA quantification, RSEM [56] was employed to
758 normalize raw read counts, transforming them into TPM (transcripts per million) values,
759 providing a relative expression level that is theoretically comparable across samples. The
760 magnitude (log2-transformed fold change) and significance (P-value) of differential expression
761 between groups were then calculated. Differentially expressed genes (DEGs) were selected
762 based on the criteria of a p-value < 0.05 and $|\log2 \text{ fold change}| \geq 1$. Gene set enrichment analysis

763 (GSEA) [57], focused on Gene Ontology[58], was conducted using the R 4.3.1 Bioconductor
764 package clusterProfiler[59] to elucidate whole transcriptomic patterns between groups. To
765 account for multiple testing, P-values underwent adjustment through the Benjamini-Hochberg
766 false discovery rate (BH-FDR).
767
768 **Single-cell RNA-seq data analysis**
769 After checking the reads quality, the sequencing files were aligned to reference human genome
770 (version GRCh38) using 10X Genomics CellRanger software (v7.1.0) count pipeline to remove
771 non-cellular barcodes and keep the cellular barcodes and gene matrix. To further distinguish
772 the Cas13bt3-valid and -invalid cells, FASTX-toolkit [60] was used to keep the reads with cellular
773 barcodes and convert FASTAQ file into FASTA file. Then, Blastn [61] was used to compute the
774 similarity between cellular reads and Cas13bt3 reference sequence.
775 Based on the quality of the sequencing reads, appropriate cutoff values for both the percentage
776 of identical positions and the alignment length were employed to delineate cells as either
777 Cas13bt3-valid or Cas13bt3-invalid. For either Cas13bt3-valid or -invalid cells, we further
778 used Seurat v4.3 for data pre-processing, data normalization, feature selection, data scaling,
779 dimensional reduction and clustering. To refine the characterization of cell types within each
780 cluster, ScType [62] was employed, leveraging genesets specific to eight retinal cell types—
781 amacrine, bipolar, cones, horizontal, macroglial, microglial, rods, and RPE—validated by Kim
782 et al. [27]. The magnitude (log2-transformed fold change) and significance (P-value) of
783 differential expression between cell types were then calculated. Differentially expressed genes
784 (DEGs) were selected based on the criteria of a p-value < 0.05 and $|\log2 \text{ fold change}| \geq 1$. Gene
785 set enrichment analysis (GSEA) [57], focused on Gene Ontology [58], was conducted using the R
786 4.3.1 Bioconductor package clusterProfiler [59] to elucidate whole transcriptomic patterns

787 between groups. To account for multiple testing, P-values underwent adjustment through the
788 Benjamini-Hochberg false discovery rate (BH-FDR).
789
790 **Statistical analysis**
791 To assess the strength of the relationship between gene expression values and the number of
792 Cas13bt3-valid read counts following log2 transformation in each cell type, Spearman's rank
793 correlation coefficient was employed. The associated *p-value* serves as an indicator of the
794 likelihood or probability that any observed correlation is merely a result of chance.
795

Acknowledgements

The authors would like to thank Liuhui Huang, Jesse Gardner-Russell and Yujie Wang for their assistance with retinal dissections, Prof Alex Hewitt and Dr Leilei Tu for providing resources for vector construction. The authors also extend their gratitude to the Vector and Genome Engineering Facility (VGEF) and the Single Cell Analytics Facility at the Children's Medical Research Institute (CMRI) for producing AAV vectors and the scRNA-seq experiments respectively and Azenta Life Sciences for conducting RNA sequencing. Schematic in figures were designed using Biorender.com.

Funding

This work was supported by grants from the National Health and Medical Research Council of Australia (NHMRC; GNT1185600), CERA Innovation Fund, National Natural Science Foundation of China (No. 82201227), and Natural Science Foundation of Guangdong Province, China (No. 2023A1515011225). Anai Gonzalez Cordero is an Al & Val Rosenstrauss Fellow (Rebecca Cooper Foundation). Funds supporting this work included the Medical Research Future Fund Stem Cell Mission (MRFF; MRF2008912), and the National Stem Cell Foundation - Metcalf Award Prize (No 00339). Satheesh Kumar was supported by the Melbourne Research Scholarship and Graeme Clark Institute Top-Up Scholarship. The Centre for Eye Research Australia receives Operational Infrastructure Support from the Victorian Government.

Author contributions

Satheesh Kumar: Conceptualization, Methodology, Formal analysis, Investigation, Data curation, Writing – original draft, Writing – review and editing. **Yi-Wen Hsiao**: Methodology,

Formal analysis, Investigation, Writing – review and editing. **Vickie H Y Wong**: Methodology, Investigation. **Deborah Aubin**: Methodology, Investigation. **Jiang-Hui Wang**: Formal analysis, Investigation. **Leszek Lisowski:** Resources. **Elizabeth Rakoczy:** Resources. **Fan Li**: Resources. **Luis Alarcon-Martinez**: Methodology. **Anai Gonzalez-Cordero**: Methodology, Investigation, Resources, Writing – review and editing, Funding acquisition. **Bang V. Bui**: Methodology, Formal analysis, Investigation, Writing – review & editing. **Guei-Sheung Liu**: Conceptualization, Methodology, Formal analysis, Resources, Data curation, Writing – original draft, Writing – review and editing, Project administration, Funding acquisition, Supervision.

Competing interests

The authors declare that they have no known competing financial interests.

Data and materials availability

RNA sequencing data generated from this study will be deposited in GEO and SRA. Other data generated during and/or analysed during the current study will be available from the corresponding author on reasonable request. Supporting data and source data can also be found in the supplementary files.

REFERENCES

1. Wang JY, Doudna JA. CRISPR technology: A decade of genome editing is only the beginning. *Science* **379**, eadd8643 (2023).

2. Kumar S*, et al.* RNA-targeting strategies as a platform for ocular gene therapy. *Prog Retin Eye Res* **92**, 101110 (2023).

3. Hu Y*, et al.* Metagenomic discovery of novel CRISPR-Cas13 systems. *Cell Discovery* **8**, 107 (2022).

4. Zhou C*, et al.* CasRx-mediated RNA targeting prevents choroidal neovascularization in a mouse model of age-related macular degeneration. *Natl Sci Rev* **7**, 835-837 (2020).

5. Zhou H*, et al.* Glia-to-Neuron Conversion by CRISPR-CasRx Alleviates Symptoms of Neurological Disease in Mice. *Cell* **181**, 590-603.e516 (2020).

6. Zheng Z*, et al.* Preventing autosomal-dominant hearing loss in Bth mice with CRISPR/CasRx-based RNA editing. *Signal Transduction and Targeted Therapy* **7**, 79 (2022).

7. Powell JE*, et al.* Targeted gene silencing in the nervous system with CRISPR-Cas13. *Science Advances* **8**, eabk2485 (2022).

8. Li Y*, et al.* Collateral cleavage of 28s rRNA by RfxCas13d causes death of mice. *bioRxiv*, 2022.2001.2017.476700 (2022).

9. Shi P*, et al.* RNA-guided cell targeting with CRISPR/RfxCas13d collateral activity in human cells. *bioRxiv*, 2021.2011.2030.470032 (2021).

10. Bot JF, van der Oost J, Geijsen N. The double life of CRISPR–Cas13. *Current Opinion in Biotechnology* **78**, 102789 (2022).

11. Xu C*, et al.* Programmable RNA editing with compact CRISPR–Cas13 systems from uncultivated microbes. *Nat Methods* **18**, 499–506 (2021).

12. Kannan S*, et al.* Compact RNA editors with small Cas13 proteins. *Nature Biotechnology*, 1-4 (2021).

13. Tong H, *et al.* High-fidelity Cas13 variants for targeted RNA degradation with minimal collateral effects. *Nature Biotechnology*, (2022).

14. Li G, *et al.* Mini-dCas13X–mediated RNA editing restores dystrophin expression in a humanized mouse model of Duchenne muscular dystrophy. *The Journal of Clinical Investigation* **133**, (2023).

15. Xiao Q, *et al.* Rescue of autosomal dominant hearing loss by in vivo delivery of mini dCas13X-derived RNA base editor. *Sci Transl Med* **14**, eabn0449 (2022).

16. Deng X, *et al.* Structural basis for the activation of a compact CRISPR-Cas13 nuclease. *Nature Communications* **14**, 5845 (2023).

17. Lin F-L, *et al.* Gene Therapy Intervention in Neovascular Eye Disease: A Recent Update. *Mol Ther* **28**, 2120-2138 (2020).

18. Xu M, Fan R, Fan X, Shao Y, Li X. Progress and Challenges of Anti-VEGF Agents and Their Sustained-Release Strategies for Retinal Angiogenesis. *Drug Des Devel Ther* **16**, 3241-3262 (2022).

19. Chuang Y-F, Wang P-Y, Kumar S, Lama S, Lin F-L, Liu G-S. Methods for in vitro CRISPR/CasRx-Mediated RNA Editing. *Frontiers in Cell and Developmental Biology* **9**, (2021).

20. Li Z, *et al.* Intrinsic targeting of host RNA by Cas13 constrains its utility. *Nature Biomedical Engineering*, (2023).

21. Li Y, *et al.* The collateral activity of RfxCas13d can induce lethality in a RfxCas13d knock-in mouse model. *Genome Biol* **24**, 20 (2023).

22. Ofer K, Benjamin BL, Owen RSD, Aartjan JWtV, Cameron M. RNA structure modulates Cas13 activity and enables mismatch detection. *bioRxiv*, 2023.2010.2005.560533 (2023).

23. Lancaster MA, Knoblich JA. Organogenesis in a dish: Modeling development and disease using organoid technologies. *Science* **345**, 1247125 (2014).

24. Wahle P, *et al.* Multimodal spatiotemporal phenotyping of human retinal organoid development. *Nature Biotechnology*, (2023).

25. Maryna VI, *et al.* PCDH15 Dual-AAV Gene Therapy for Deafness and Blindness in Usher Syndrome Type 1F. *bioRxiv*, 2023.2011.2009.566447 (2023).

26. West EL, *et al.* Antioxidant and lipid supplementation improve the development of photoreceptor outer segments in pluripotent stem cell-derived retinal organoids. *Stem Cell Reports* **17**, 775-788 (2022).

27. Kim HJ, *et al.* Comprehensive characterization of fetal and mature retinal cell identity to assess the fidelity of retinal organoids. *Stem Cell Reports* **18**, 175-189 (2023).

28. Hu H, Sun S-C. Ubiquitin signaling in immune responses. *Cell Research* **26**, 457-483 (2016).

29. Rakoczy EP, *et al.* Characterization of a mouse model of hyperglycemia and retinal neovascularization. *Am J Pathol* **177**, 2659-2670 (2010).

30. Nakagawa R, *et al.* Structure and engineering of the minimal type VI CRISPR-Cas13bt3. *Molecular Cell* **82**, 3178-3192.e3175 (2022).

31. Nishijima K, *et al.* Vascular Endothelial Growth Factor-A Is a Survival Factor for Retinal Neurons and a Critical Neuroprotectant during the Adaptive Response to Ischemic Injury. *Am J Pathol* **171**, 53-67 (2007).

32. Le Y-Z. VEGF production and signaling in Müller glia are critical to modulating vascular function and neuronal integrity in diabetic retinopathy and hypoxic retinal vascular diseases. *Vision Research* **139**, 108-114 (2017).

33. Ford KM, Saint-Geniez M, Walshe T, Zahr A, D'Amore PA. Expression and Role of VEGF in the Adult Retinal Pigment Epithelium. *Investigative Ophthalmology & Visual Science* **52**, 9478-9487 (2011).

34. Colognori D, Trinidad M, Doudna JA. Precise transcript targeting by CRISPR-Csm complexes. *Nature Biotechnology* **41**, 1256-1264 (2023).

35. Jo N, *et al.* Inhibition of Platelet-Derived Growth Factor B Signaling Enhances the Efficacy of Anti-Vascular Endothelial Growth Factor Therapy in Multiple Models of Ocular Neovascularization. *Am J Pathol* **168**, 2036-2053 (2006).

36. Park J, *et al.* CRISPR/Cas9 mediated specific ablation of vegfa in retinal pigment epithelium efficiently regresses choroidal neovascularization. *Sci Rep* **13**, 3715 (2023).

958 37. Garita-Hernandez M, *et al.* AAV-Mediated Gene Delivery to 3D Retinal Organoids
959 Derived from Human Induced Pluripotent Stem Cells. *Int J Mol Sci* **21**, (2020).

960
961 38. McClements ME, *et al.* Tropism of AAV Vectors in Photoreceptor-Like Cells of
962 Human iPSC-Derived Retinal Organoids. *Translational Vision Science & Technology*
963 **11**, 3-3 (2022).

964
965 39. Duong TT, *et al.* Comparative AAV-eGFP Transgene Expression Using Vector
966 Serotypes 1–9, 7m8, and 8b in Human Pluripotent Stem Cells, RPEs, and Human and
967 Rat Cortical Neurons. *Stem Cells International* **2019**, 7281912 (2019).

968
969 40. Eoi Jong S, Jeong AC, Jae-Young K, Young Hee Y. Aflibercept ameliorates retinal
970 pericyte loss and restores perfusion in streptozotocin-induced diabetic mice. *BMJ Open*
971 *Diabetes Research & Care* **8**, e001278 (2020).

972
973 41. Tokunaga CC, *et al.* Effects of Anti-VEGF Treatment on the Recovery of the
974 Developing Retina Following Oxygen-Induced Retinopathy. *Investigative*
975 *Ophthalmology & Visual Science* **55**, 1884-1892 (2014).

976
977 42. Shah CP, Garg SJ, Vander JF, Brown GC, Kaiser RS, Haller JA. Outcomes and Risk
978 Factors Associated with Endophthalmitis after Intravitreal Injection of Anti-Vascular
979 Endothelial Growth Factor Agents. *Ophthalmology* **118**, 2028-2034 (2011).

980
981 43. Lai AKW, Lo ACY. Animal Models of Diabetic Retinopathy: Summary and
982 Comparison. *Journal of Diabetes Research* **2013**, 106594 (2013).

983
984 44. Smith LEH, *et al.* Regulation of vascular endothelial growth factor-dependent retinal
985 neovascularization by insulin-like growth factor-1 receptor. *Nat Med* **5**, 1390-1395
986 (1999).

987
988 45. Huang X, *et al.* Genome editing abrogates angiogenesis in vivo. *Nature*
989 *Communications* **8**, 112 (2017).

990
991 46. Holmgaard A, *et al.* In Vivo Knockout of the Vegfa Gene by Lentiviral Delivery of
992 CRISPR/Cas9 in Mouse Retinal Pigment Epithelium Cells. *Molecular Therapy -*
993 *Nucleic Acids* **9**, 89-99 (2017).

994
995 47. Holmgaard AB, *et al.* Targeted Knockout of the Vegfa Gene in the Retina
996 by Subretinal Injection of RNP Complexes Containing Cas9 Protein and Modified
997 sgRNAs. *Mol Ther* **29**, 191-207 (2021).

998

48. Wang Y, *et al.* Efficient Human Genome Editing Using SaCas9 Ribonucleoprotein Complexes. *Biotechnology journal* **14**, e1800689 (2019).

49. Chung SH, *et al.* CRISPR-based VEGF suppression using paired guide RNAs for treatment of choroidal neovascularization. *Molecular Therapy - Nucleic Acids* **28**, 613-622 (2022).

50. Konermann S, Lotfy P, Brideau NJ, Oki J, Shokhirev MN, Hsu PD. Transcriptome Engineering with RNA-Targeting Type VI-D CRISPR Effectors. *Cell* **173**, 665-676.e614 (2018).

51. Lai C-M. Generation of transgenic mice with mild and severe retinal neovascularisation. *Br J Ophthalmol* **89**, 911-916 (2005).

52. Zudaire E, Gambardella L, Kurcz C, Vermeren S. A Computational Tool for Quantitative Analysis of Vascular Networks. *PLoS One* **6**, e27385 (2011).

53. Andrews S. FastQC: a quality control tool for high throughput sequence data.). Babraham Bioinformatics, Babraham Institute, Cambridge, United Kingdom (2010).

54. Bolger AM, Lohse M, Usadel B. Trimmomatic: a flexible trimmer for Illumina sequence data. *Bioinformatics* **30**, 2114-2120 (2014).

55. Dobin A, *et al.* STAR: ultrafast universal RNA-seq aligner. *Bioinformatics* **29**, 15-21 (2013).

56. Li B, Dewey CN. RSEM: accurate transcript quantification from RNA-Seq data with or without a reference genome. *BMC bioinformatics* **12**, 1-16 (2011).

57. Hung J-H, Yang T-H, Hu Z, Weng Z, DeLisi C. Gene set enrichment analysis: performance evaluation and usage guidelines. *Briefings in bioinformatics* **13**, 281-291 (2012).

58. Consortium GO. The Gene Ontology (GO) database and informatics resource. *Nucleic acids research* **32**, D258-D261 (2004).

59. Yu G, Wang L-G, Han Y, He Q-Y. clusterProfiler: an R package for comparing biological themes among gene clusters. *Omics: a journal of integrative biology* **16**, 284-287 (2012).

1039 60. Gordon A, Hannon GJ. Fastx-toolkit. *FASTQ/A short-reads preprocessing tools*
1040 *(unpublished) http://hannonlab cshl edu/fastx_toolkit* **5**, (2010).

1041
1042 61. Ye J, McGinnis S, Madden TL. BLAST: improvements for better sequence analysis.
1043 *Nucleic acids research* **34**, W6-W9 (2006).

1044
1045 62. Ianevski A, Giri AK, Aittokallio T. Fully-automated and ultra-fast cell-type
1046 identification using specific marker combinations from single-cell transcriptomic data.
1047 *Nature communications* **13**, 1246 (2022).

1048
1049 63. Limb GA, Salt TE, Munro PM, Moss SE, Khaw PT. In vitro characterization of a
1050 spontaneously immortalized human Müller cell line (MIO-M1). *Invest Ophthalmol Vis*
1051 *Sci* **43**, 864-869 (2002).

1052
1053 64. Love MI, Huber W, Anders S. Moderated estimation of fold change and dispersion for
1054 RNA-seq data with DESeq2. *Genome Biol* **15**, 550 (2014).

1055
1056 65. Hao Y*, et al.* Dictionary learning for integrative, multimodal and scalable single-cell
1057 analysis. *Nature Biotechnology*, (2023).

1058

1059

1060

1061 Key Resources Table

Reagent or Resource	Source	Identifier
Chemicals		
DMEM	Thermo Fisher Scientific	Cat# 11965092
DMEM/F12	Thermo Fisher Scientific	Cat# 11320033
Opti-MEM	Thermo Fisher Scientific	Cat# 31985070
TrypLE™ Express	Thermo Fisher Scientific	Cat# 12605093
GlutaMAX™ Supplement	Thermo Fisher Scientific	Cat# 35050061
FBS	Bovogen Biologicals	SFBS-AU
Antibiotic-Antimycotic	Thermo Fisher Scientific	Cat# 15240062
DPBS	Thermo Fisher Scientific	Cat# 14190250
Lipofectamine™ 3000 Transfection Reagent	Thermo Fisher Scientific	Cat# L3000001
ViaFect™ Transfection Reagent	Promega Corporation	Cat# E4982
NEB® Stable Competent E. coli, High Efficiency	New England Biolabs	Cat# C3040I
rCutSmart™ Buffer	New England Biolabs	Cat# B6004S
NEB® 10-beta/Stable Outgrowth Medium	New England Biolabs	Cat# B9035S
NucBlue™ Live ReadyProbes™ Reagent (Hoechst 33342)	Thermo Fisher Scientific	Cat# R37605
LB (Lennox L) agar	Thermo Fisher Scientific	Cat# 22700025
2-YT Broth	Thermo Fisher Scientific	Cat# 22712020

Carbenicillin Disodium Salt	Thermo Fisher Scientific	Cat# 10177012
GelRed® nucleic acid gel stain	Biotium	Cat# 41003
Phosphate buffered saline	Merck	Cat# P3813
Tween-20	Merck	Cat# P1379
Triton-X-100	Amresco	Cat# 0694
RIPA Lysis and Extraction Buffer	Thermo Fisher Scientific	Cat# 89900
Pierce™ Phosphatase Inhibitor Mini Tablets	Thermo Fisher Scientific	Cat# A32957
NuPAGE™ MES SDS Running Buffer (20X)	Thermo Fisher Scientific	Cat# NP0002
NuPAGE™ LDS Sample Buffer (4X)	Thermo Fisher Scientific	Cat# NP0007
0.5% Proxymethacaine hydrochloride (Alcaine™)	Alcon	N/A
0.5% Tropicamide (Mydriacyl)	Alcon	N/A
GenTeal™ Gel	Alcon	N/A
Ketamine, 100 mg/mL	Troy Laboratories	Ketamil
Xylazine, 100 mg/mL	Troy Laboratories	Ilium Xylazil-100
Experimental models: Cell lines		
Human: HEK293FT	Thermo Fisher Scientific	R70007
Human: ARPE-19	ATCC	CRL-2302™
Human: Müller 1 (MIO-M1)	UCL Institute of Ophthalmology, London	[63]
Experimental models: Organisms/ strains		

Human: 3D retinal organoid	Children's Medical Research Institute	[27]
Kimba Mouse	The University of Western Australia	[29]
Antibodies		
Mouse anti-actin, clone C4	Merck	MAB1501
Rabbit anti-HA, C29F4	Cell Signaling Technology	#3724
Mouse anti-rhodopsin, 1D4	Abcam	ab5417
Rat mCherry monoclonal 16D7, Alexa Fluor™ 594	Thermo Fisher Scientific	Cat# M11240
Rat anti-laminin monoclonal, α-2 chain	Merck	L0663
Donkey anti-rat AffiniPure Fragment IgG (H + L), Alexa Fluor™ 647	Jackson ImmunoResearch	712-606-150
Donkey mouse AffiniPure Fragment IgG (H + L), Alexa Fluor™	Jackson ImmunoResearch	715-546-151
Goat anti-rabbit IgG (H+L) Secondary Antibody, HRP	Thermo Fisher Scientific	Cat# 31460
Goat anti-Mouse IgG (H+L) Secondary Antibody, HRP	Thermo Fisher Scientific	Cat# 62-6520
Anti-Arrestin C antibody, C-terminal	Abcam	189437
Monoclonal Anti-Opsin antibody produced in mouse	Merck	O4886

Sheep anti Human chx 10 (Visual system homeobox 2) (NT)	ExAlpha	XII80P
CRALBP Monoclonal Antibody (B2)	Thermo Fisher Scientific	MA1-813
Anti-Prox 1 Antibody	Merck	AB5475
HuC/HuD Monoclonal Antibody (16A11)	Thermo Fisher Scientific	A21271
Commercial kits		
RNeasy Mini kit	Qiagen	Cat# 74106
Monarch® Total RNA Miniprep Kit	New England Biolabs	Cat# T2010S
High-Capacity cDNA Reverse Transcription Kit	Thermo Fisher Scientific	Cat# 4368814
Q5® Hot Start High-Fidelity Master Mix	New England Biolabs	Cat# M0494S
TaqMan™ Fast Advanced Master Mix	Thermo Fisher Scientific	Cat# 4444557
SYBR™ Green PCR Master Mix	Thermo Fisher Scientific	Cat# 4309155
Human VEGF DuoSet ELISA	R & D systems	Cat# DY293B
Recombinant DNA		
pAAV.CMV-CasRx mCh	Addgene	203442
pAAV.CMV-CasRx-VEGFA sgRNA	Addgene	203443
pAAV.CMV-CasRx-VEGFA sgRNA array	Addgene	203444
pAAV.CMV-Cas13bt3-NT sgRNA	Addgene	203446

pAAV.CMV-Cas13bt3-VEGFA sgRNA	Addgene	203447
pAAV.CMV-Cas13bt3-VEGFA sgRNA array	Addgene	203448
pAAV.CMV-Cas13bt3 (GenScript CO)-NT sgRNA	Addgene	203451
pAAV.CMV-Cas13bt3 (GenScript CO)-VEGFA sgRNA	Addgene	203452
Software and algorithms		
GraphPad Prism 10	GraphPad	https://www.graphpad.com/scientific-software/prism/E/
Benchling	Benchling	https://www.benchling.com/
Fiji-ImageJ	National Institutes of Health	https://imagej.net/software/fiji/
GenSmart™ Codon Optimisation	GenScript	https://www.genscript.com/gensmart-free-gene-codon-optimization.html
IDT Codon Optimisation Tool	Integrated DNA Technologies	https://sg.idtdna.com/pages/tools/codon-optimization-tool
STAR (2.7.11a)	[55]	https://github.com/alexdobin/STAR
DESeq2 (v3.18)	[64]	https://bioconductor.org/packages/release

		/bioc/html/DESeq2.html
Seurat (v5)	[65]	https://satijalab.org/seurat/
Cell Ranger (v7.2)	10X Genomics	https://www.10xgenomics.com/support/software/cell-ranger
ImageLab (v6.1)	Bio-Rad	https://www.bio-rad.com/en-au/product/image-lab-software
R (v4.3.2)	R Core Team	https://cran.r-project.org/
RStudio (v2023.09.1)	Posit PBC	https://posit.co/download/rstudio-desktop/
Adobe Photoshop (v25)	Adobe Inc.	https://www.adobe.com/au/products/photoshop.html
AngioTool (v0.5)	National Cancer Institute	https://ccrod.cancer.gov/confluence/display/ROB2/Downloads
Equipment		
HRA + OCT Spectralis	Heidelberg Engineering	N/A
Leica Stellaris 5 confocal microscope	Leica Microsystems	N/A

1062

1063 **Primers used in this study.**

Quantitative PCR		
Name	**Source**	**Identifier**
Human VEGFA (Hs00900055_m1)	Thermo Fisher Scientific	Cat# 4331182
Mouse VEGFA (Mm00437306_m1)	Thermo Fisher Scientific	Cat# 4331182
Human GAPDH (Hs02786624_g1)	Thermo Fisher Scientific	Cat# 4448489
Mouse GAPDH (Mm99999915_g1)	Thermo Fisher Scientific	Cat# 4448489
Standard PCR		
Name	**Sequence (5' - 3')**	**Source**
Cas13bt3_FWD	CGGCGAACAGGGTGATAAA	Integrated DNA Technologies
Cas13bt3_REV	CTGTGCTGGGCTTCAAGATA	Integrated DNA Technologies

1064

1065

1066

1067

1068

1069

1070 **SUPPLEMENTARY DATA**

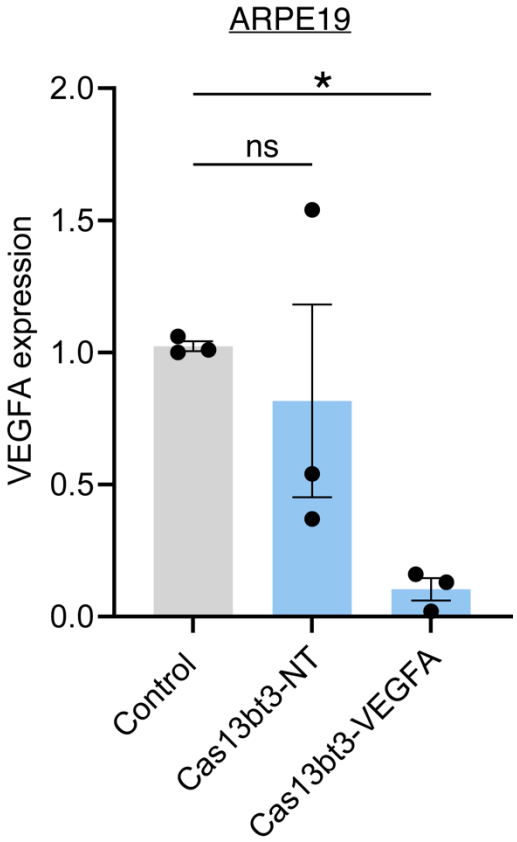

1071

1072 **Supplementary figure 1. Evaluation of Cas13bt3 targeting in retinal cell lines.** VEGFA
1073 mRNA expression in ARPE19 cells following transfection of control, Cas13bt3-NT and
1074 Cas13bt3-VEGFA. A significant reduction in Cas13bt3-VEGFA was observed. Data presented
1075 as mean ± SEM. ns: not significant. *P≤0.05.

1076

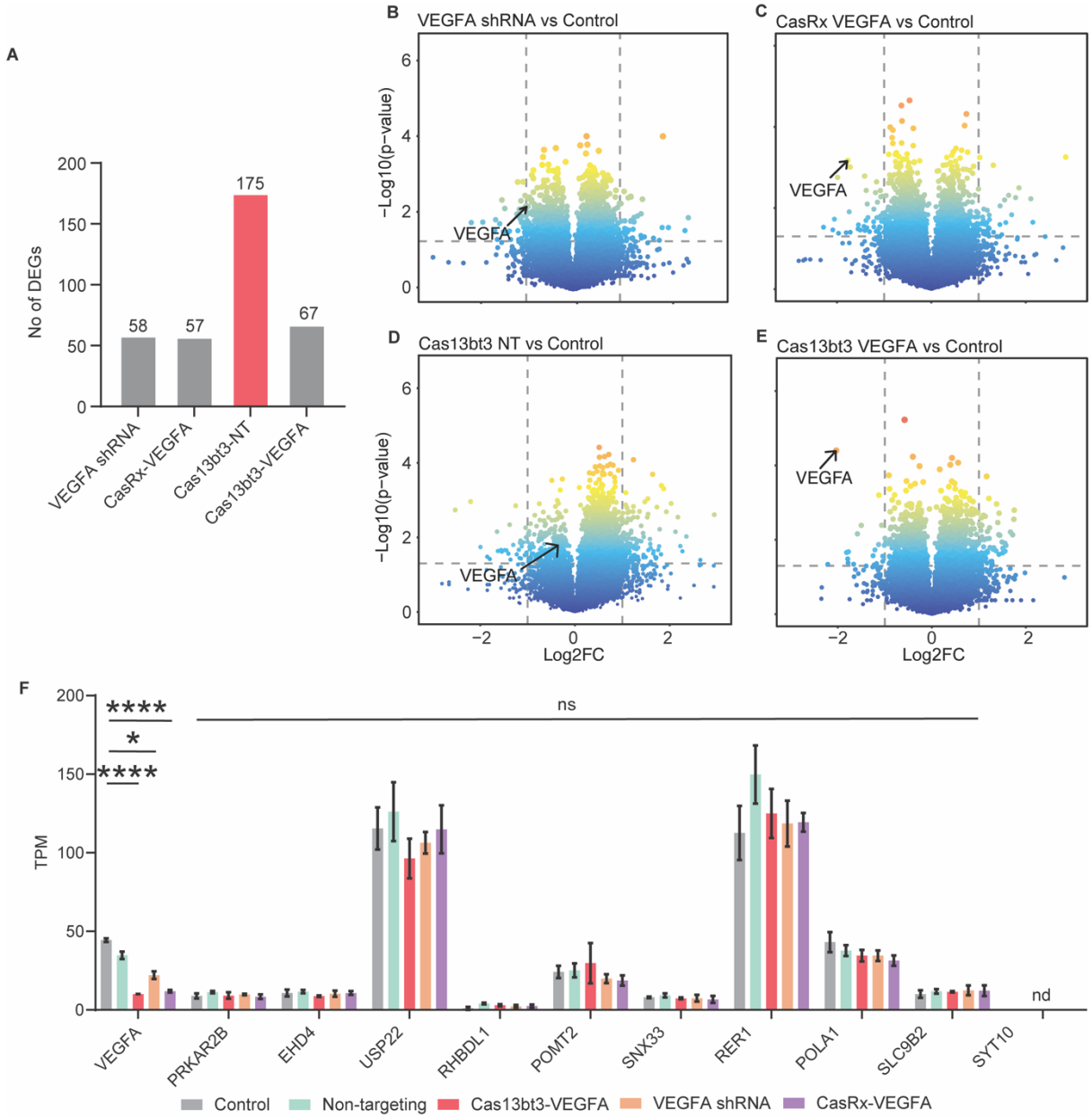

Supplementary figure 2. HEK293FT DEG and off target analysis. (A) Number of differentially expressed genes from the VEGFA-targeting shRNA, CasRx and Cas13bt3 transfections in HEK293FT cells compared to vector control. **(B)** Volcano plots of differentially expressed genes from VEGFA shRNA, **(C)** CasRx VEGFA sgRNA, **(D)** Cas13bt3 NT sgRNA and **(E)** Cas13bt3 VEGFA sgRNA compared to vector control. **(F)** Plot of TPM values for VEGFA and candidate off-target genes from Cas13bt3-NT sgRNA and Cas13bt3 VEGFA sgRNA groups compared to shRNA and CasRx targeting vectors. Statistical analysis was conducted by Welch's t test **(F)**. Data presented as mean ± SEM. ns: not significant. *P≤0.05, ****P≤0.00001.

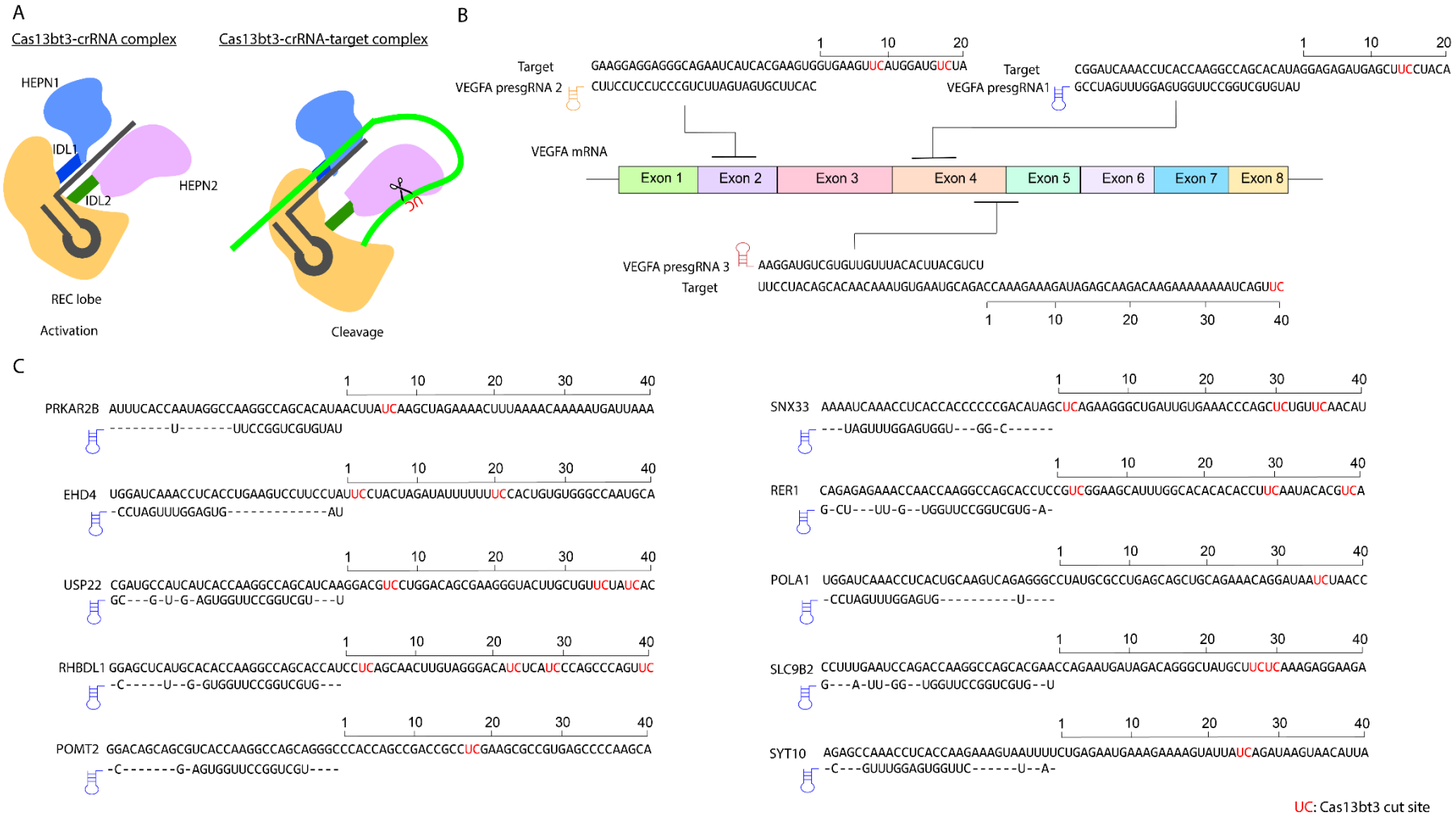
A
Cas13bt3-crRNA complex
Cas13bt3-crRNA-target complex
HEPN1
IDL1
IDL2
HEPN2
REC lobe
Activation
Cleavage
B
Target
GAAGGAGGAGGGCAGAAUCAUCACGAAGUGGUGAAGUUCAUGGAUGUCUA
VEGFA presgRNA 2
CUUCCUCCUCCCGUCUUAGUAGUGCUUCAC
Target
CGGAUCAAACCUCACCAAGGCCAGCACAUAGGAGAGAUGAGCUUCCUACA
VEGFA presgRNA1
GCCUAGUUUGGAGUGGUUCCGGUCGUGUAU
VEGFA mRNA
Exon 1
Exon 2
Exon 3
Exon 4
Exon 5
Exon 6
Exon 7
Exon 8
VEGFA presgRNA 3
AAGGAUGUCGUGUUGUUUACACUUACGUCU
Target
UUCCUACAGCACAACAAAUGUGAAUGCAGACCAAAGAAAGAUAGAGCAAGACAAGAAAAAAAAUCAGUUC
C
PRKAR2B AUUUCACCAAUAGGCCAAGGCCAGCACAUAACUUAUCAAGCUAGAAAACUUUAAAACAAAAAUGAUUAAA
--------U-------UUCCGGUCGUGUAU
EHD4 UGGAUCAAACCUCACCUGAAGUCCUUCCUAUUCCUACUAGAUAUUUUUUCCACUGUGUGGGCCAAUGCA
-CCUAGUUUGGAGUG----------AU
USP22 CGAUGCCAUCAUCACCAAGGCCAGCAUCAAGGACGUCCUGGACAGCGAAGGGUACUUGCUGUUCUAUCAC
GC---G-U-G-AGUGGUUCCGGUCGU---U
RHBDL1 GGAGCUCAUGCACACCAAGGCCAGCACCAUCCUCAGCAACUUGUAGGGACAUCUCAUCCCAGCCCAGUUC
-C-----U--G-GUGGUUCCGGUCGUG---
POMT2 GGACAGCAGCGUCACCAAGGCCAGCAGGGCCCACCAGCCGACCGCCUCGAAGCGCCGUGAGCCCCAAGCA
-C-------G-AGUGGUUCCGGUCGU----
SNX33 AAAAUCAAACCUCACCACCCCCCGACAUAGCUCAGAAGGGCUGAUUGUGAAACCCAGCUCUGUUCAACAU
---UAGUUUGGAGUGGU---GG-C------
RER1 CAGAGAGAAACCAACCAAGGCCAGCACCUCCGUCGGAAGCAUUUGGCACACACACCUUCAAUACACGUCA
G-CU---UU-G--UGGUUCCGGUCGUG-A-
POLA1 UGGAUCAAACCUCACUGCAAGUCAGAGGGCCUAUGCGCCUGAGCAGCUGCAGAAACAGGAUAAUCUAACC
-CCUAGUUUGGAGUG----------U----
SLC9B2 CCUUUGAAUCCAGACCAAGGCCAGCACGAACCAGAAUGAUAGACAGGGCUAUGCUUCUCAAAGAGGAAGA
G---A-UU-GG--UGGUUCCGGUCGUG--U
SYT10 AGAGCCAAACCUCACCAAGAAAGUAAUUUUCUGAGAAUGAAAGAAAAGUAUUAUCAGAUAAGUAACAUUA
-C---GUUUGGAGUGGUUC------U--A-
UC: Cas13bt3 cut site

1087

1088 **Supplementary figure 3. Prediction of Cas13bt3 cut sites**. **(A)** Schematic of Cas13bt3-gRNA and Cas13bt3-gRNA-target complex. **(B)** Potential
1089 Cas13bt3 cut sites on VEGFA mRNA target for VEGFA sgRNA1, 2 and 3. **(C)** Potential Cas13bt3 cut sites on top 10 candidate off-target genes
1090 for VEFGA sgRNA 1.

```
A  VEGFA        TATGTGCTGGCCTTGGTGAGGTTTGATCCG
   PRKAR2B      TATGTGCTGGCCTTGG--------------
   EHD4         ---------------GGTGAGGTTTGATCC-
   USP22        ----TGCTGGCCTTGGTGA-----------
   RHBDL1       ---GTGCTGGCCTTGGTG------------
   POMT2        ----TGCTGGCCTTGGTGA-----------
   SNX33        ---------------TGGTGAGGTTTGAT---
   RER1         ---GTGCTGGCCTTGGT-------------
   POLA1        ----------------GTGAGGTTTGATCC-
   SLC9B2       ---GTGCTGGCCTTGGT-------------
   SYT10        -----------CTTGGTGAGGTTTG-----

B  VEGFA presgRNA 2  CACTTCGTGATGATTCTGCCCTCCTCCTTC
   BARX1        ----------------TCTGCCCTCCTCCTTC
   SLX4         ----------------TCTGCCCTCCTCCTTC
   LOC 100192426 ----------------TCTGCCCTCCTCCTTC
   NRG1         --------GATGATTCTGCCCTC-------
   AGRN         -------------ATTCTGCCCTCCTCC---
   TRIM56       ----------------CTGCCCTCCTCCTTC
   CDH20        -----------GATTCTGCCCTCCTCCTTC
   MORC3        ----------TGATTCTGCCCTCCT-----
   ZNF32-AS3    ----------------CTGCCCTCCTCCTTC
   SUGT1P4-STRA6LP  CACTTCGTGATGAT----------------

C  VEGFA presgRNA 3  TCTGCATTCACATTTGTTGTGCTGTAGGAA
   NUP210L      ----------CATTTGTTGTGCTGT-----
   LOC 105373744  TCTGCATTCACATTT---------------
   LYSMD3       ----------CATTTGTTGTGCTGT-----
   SKP1         -CTGCATTCACATTTG--------------
   CPA4         --TGCATTCACATTTG--------------
   SENP5        -CTGCATTCACATTTGTT------------
```

Supplementary figure 4. Multiplexed VEGFA knockdown using Cas13bt3. (A) Top off-target genes for VEGFA sgRNA 1, **(B)** VEGFA sgRNA 2 and **(C)** VEGFA sgRNA 3.

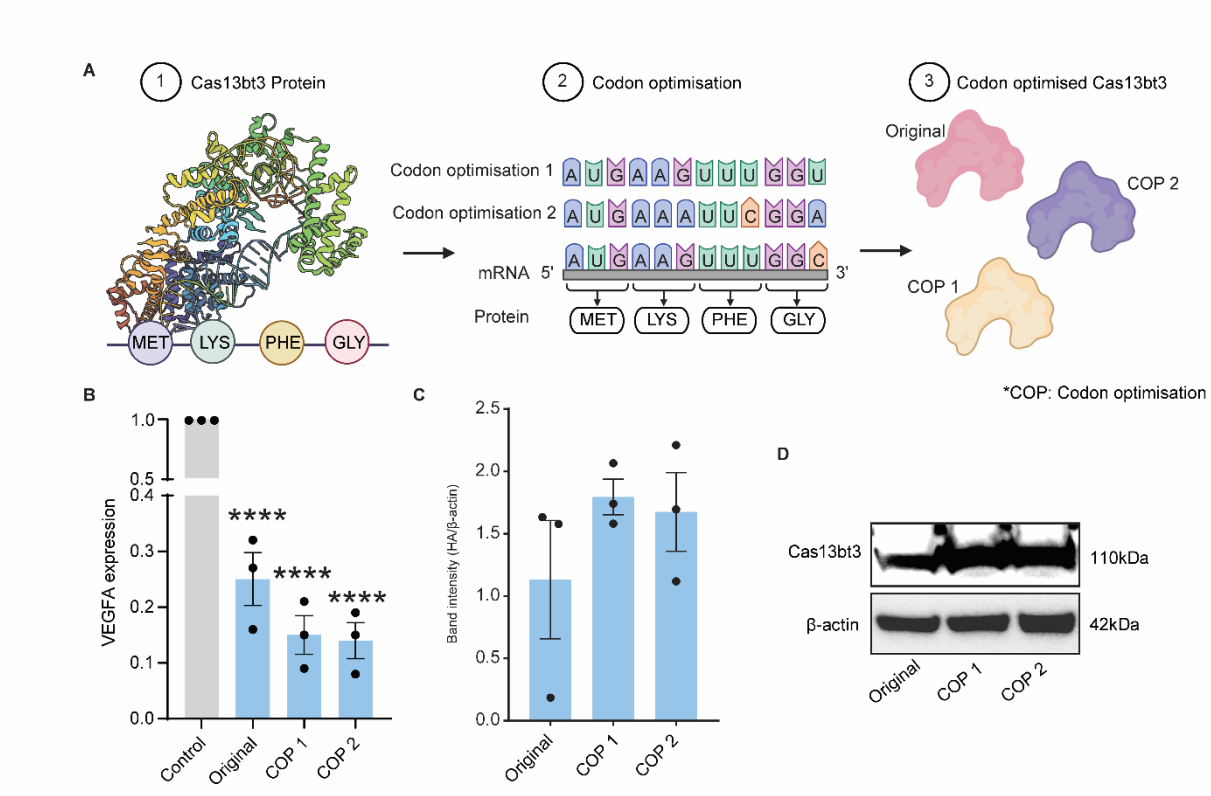

Supplementary Figure 5. Codon optimisation of Cas13bt3. (A) Schematic of codon optimisation procedure from Cas13e protein sequence. **(B)** VEGFA mRNA knockdown from original and codon optimised Cas13e compared to control transfection. **(C and D)** Expression of original and codon optimised determined from Western blot. Statistical analyses was conducted using One-way ANOVA with Tukey's multiple comparisons test (**B and C**). Data presented as mean ± SEM. *P≤0.05, **P≤0.001, ****P≤0.00001.

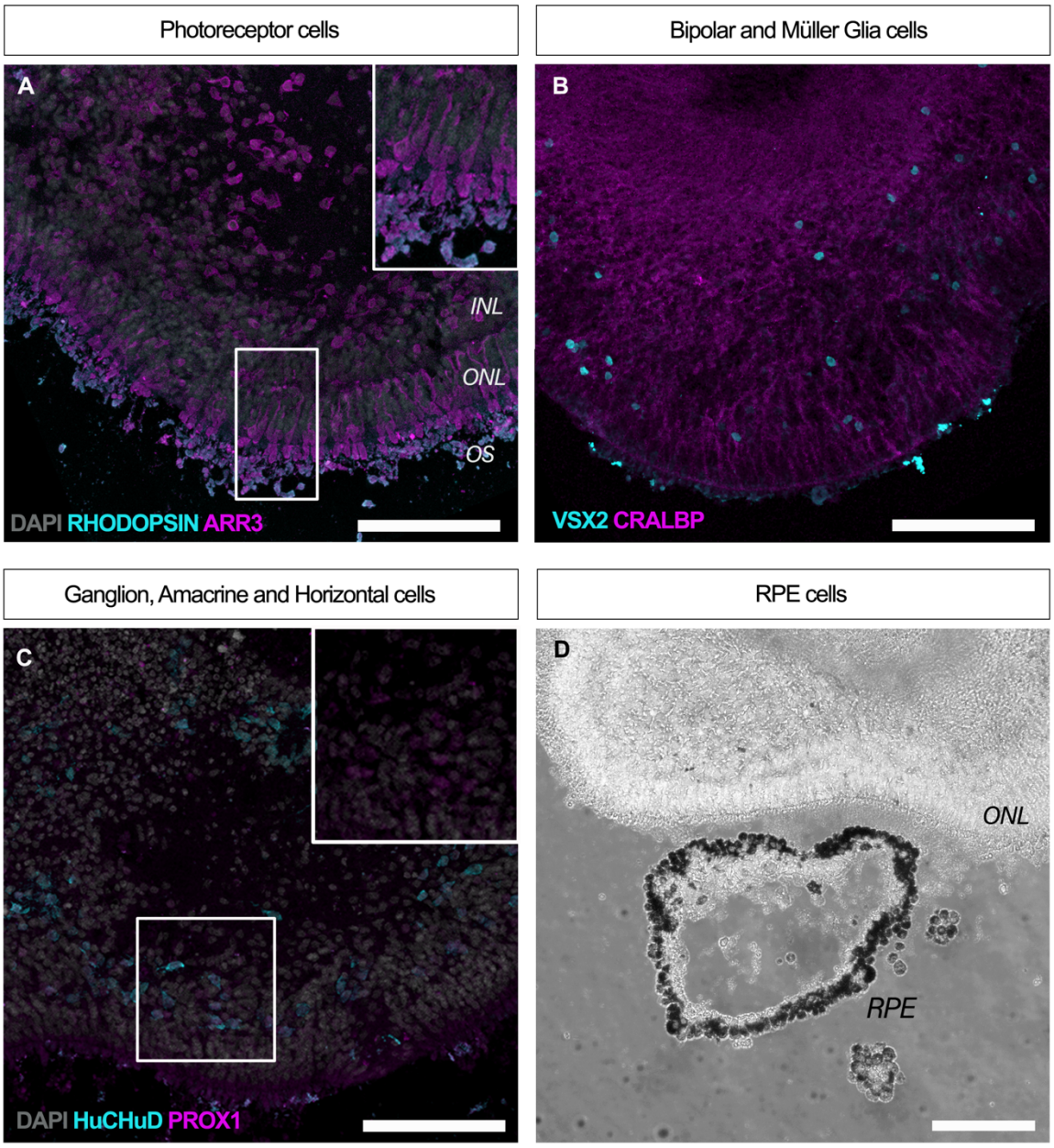

Supplementary figure 6. Characterization of 30 weeks retinal organoids. (A) Retinal organoids showed expression of mature photoreceptor markers Arrestin-3 (magenta) specific to the cone cells and Rhodopsin (cyan) localized to the outer segments (OS) of rod photoreceptor cells. **(B, C)** In the inner nuclear layer (INL) bipolar cells stained with VSX2 (cyan) and Müller glia stained with CRALBP (magenta) **(B)**, Amacrine and horizontal cells stained with PROX1 (magenta) and ganglion cells stained with HuCHuD (cyan) **(C)**. **(D)** Brightfield image of retinal organoid section showing the outer nuclear layer (ONL) and a pigmented RPE island next to it. Scale bar: 116µm. Abbreviations: INL: inner nuclear layer ONL: outer Nuclear Layer, OS: outer segment, RPE: retinal pigment epithelium.

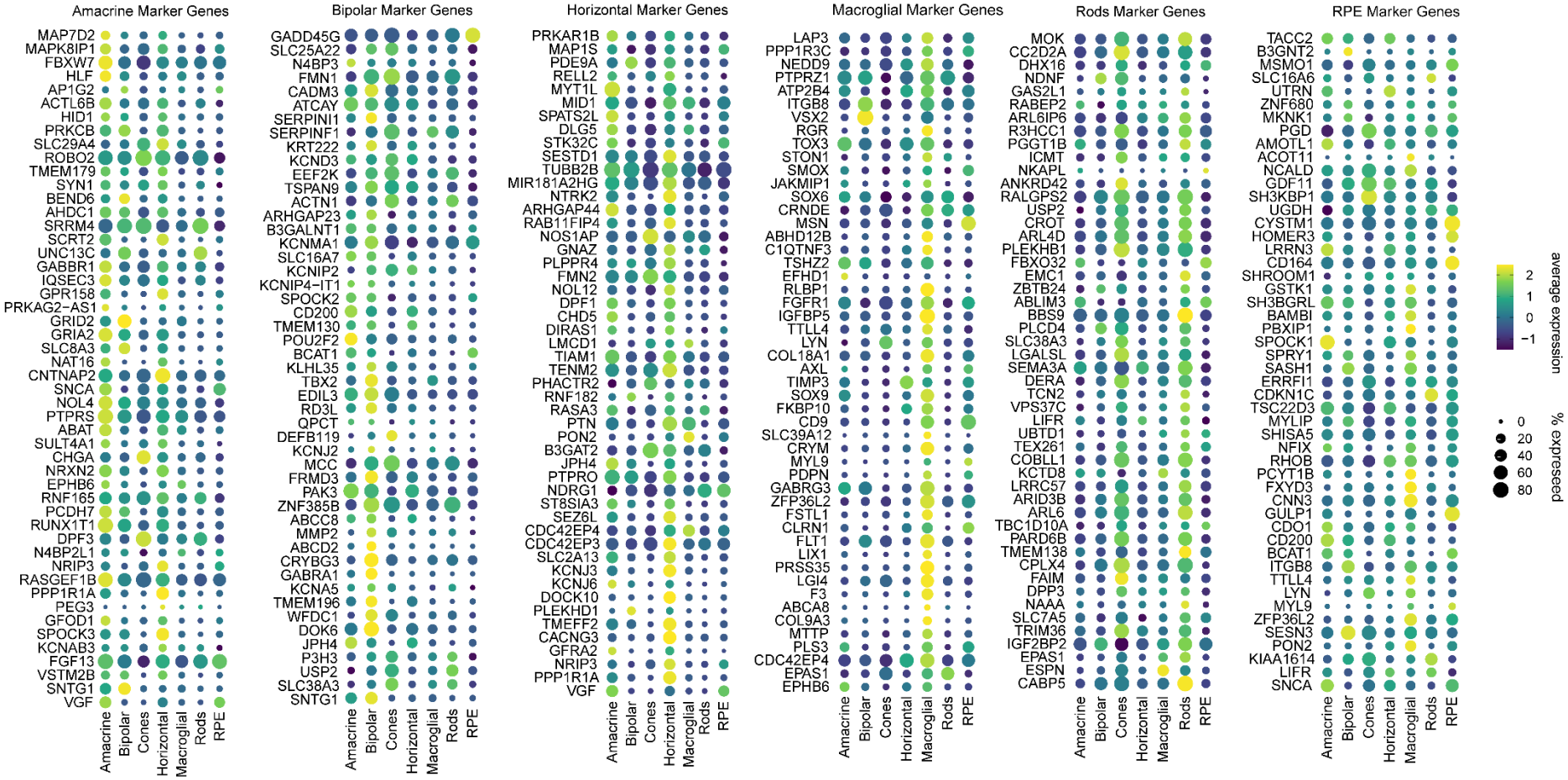

Supplementary figure 7. Dot plots of retinal cell marker genes for respective cell types in 3D retinal organoids. Complete list of cell marker genes can obtained from Kim et al., 2023 [25].

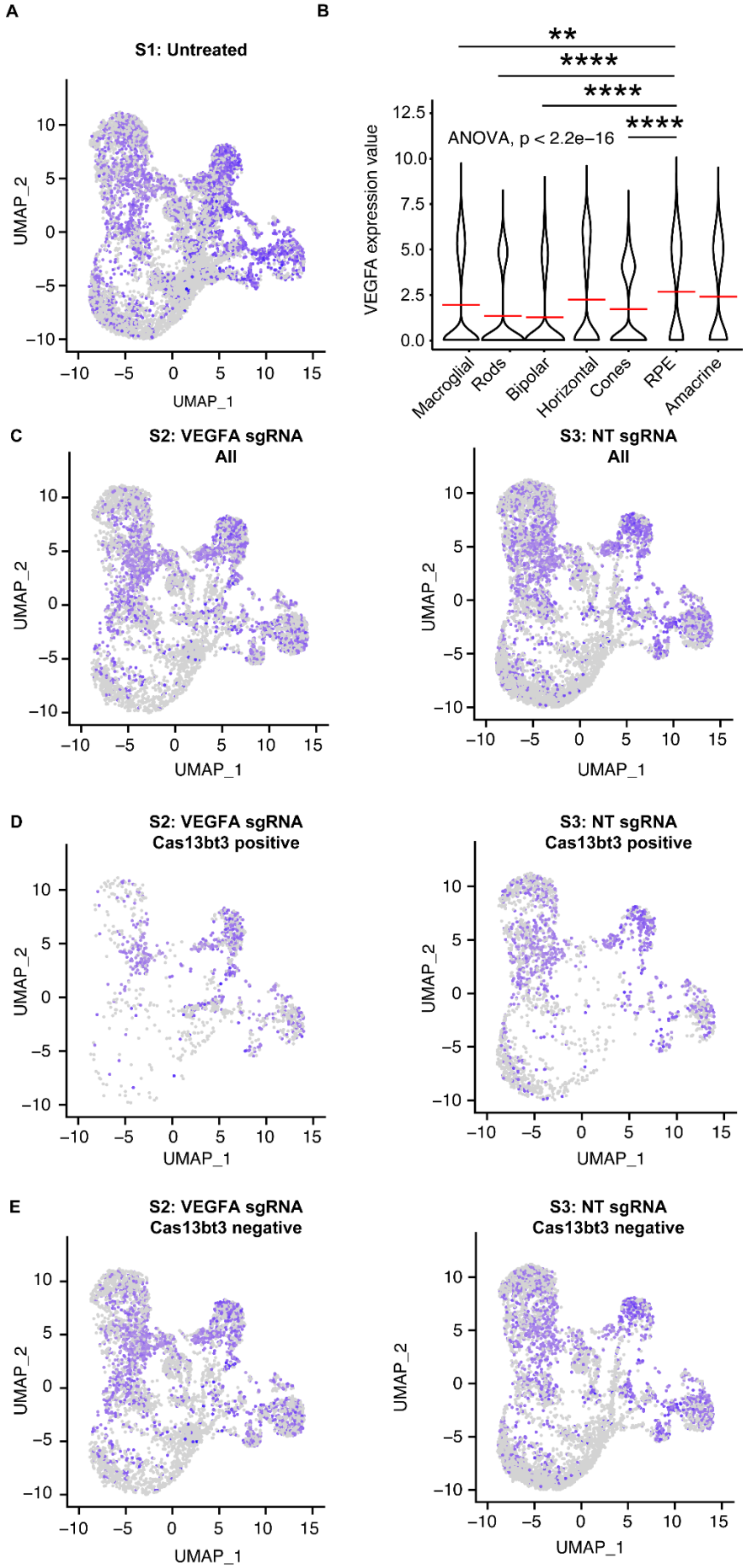
A
S1: Untreated
UMAP_2
UMAP_1
B
**
****
****
****
ANOVA, p < 2.2e−16
VEGFA expression value
Macroglial
Rods
Bipolar
Horizontal
Cones
RPE
Amacrine
C
S2: VEGFA sgRNA
All
S3: NT sgRNA
All
D
S2: VEGFA sgRNA
Cas13bt3 positive
S3: NT sgRNA
Cas13bt3 positive
E
S2: VEGFA sgRNA
Cas13bt3 negative
S3: NT sgRNA
Cas13bt3 negative

1116

1117 **Supplementary figure 8. *E*xpression of VEGFA *on* retinal cell clusters.** UMAP plots of
1118 showing expression on **(A)** Untreated retinal organoid. **(B)** Violin plots showing expression of
1119 VEGFA in individual retinal cell types. **(C)** UMAP plots of retinal cell clusters with expression
1120 of VEGFA from VEGFA-treated and NT-treated retinal organoids, **(C)** all cells, **(D)** Cas13bt3
1121 positive cells and **(E)** Cas13bt3 negative cells. Data analyses were conducted using One-way
1122 ANOVA with Tukey's multiple comparisons test (B). **P≤0.001, ****P≤0.00001.

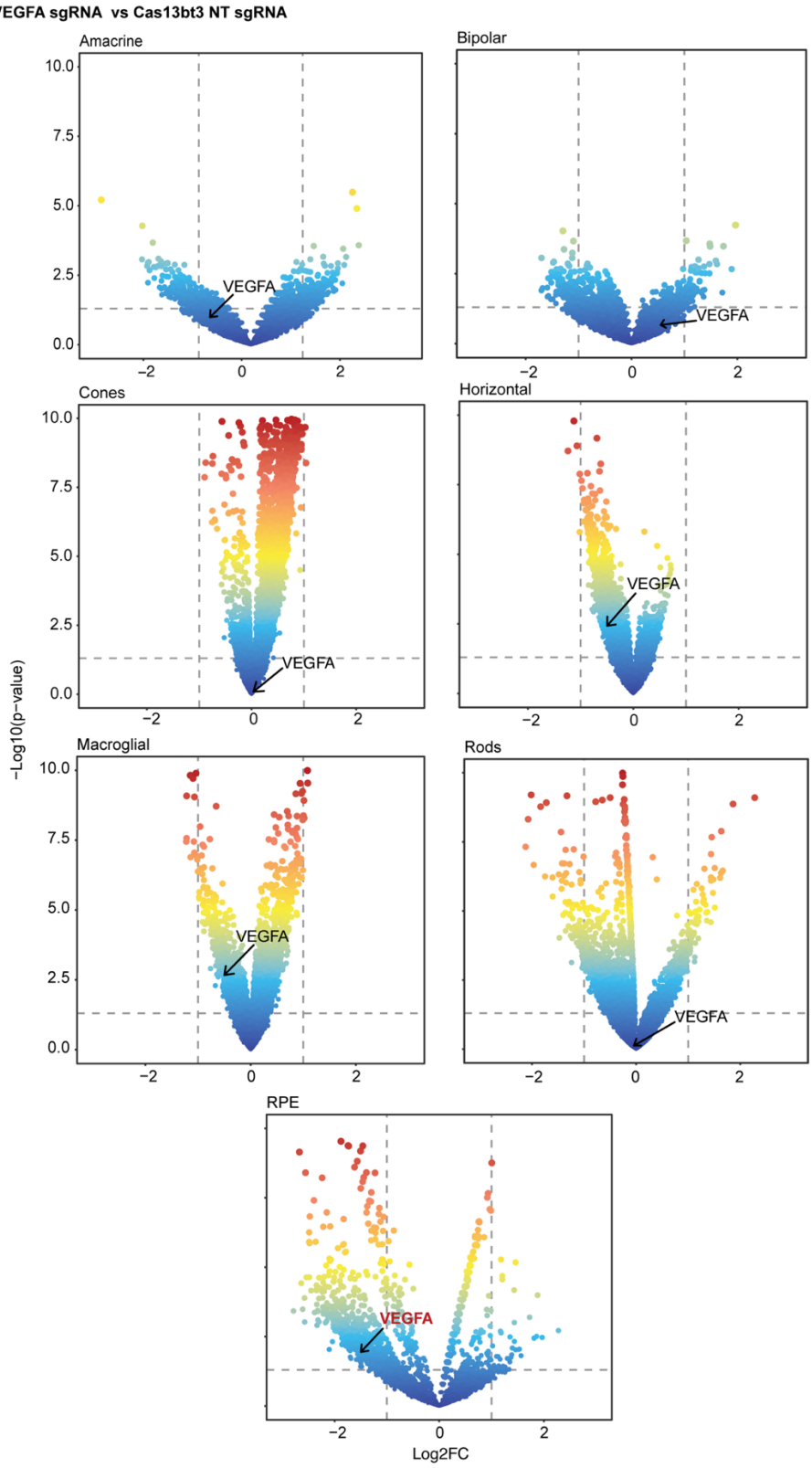

1123

1124 **Supplementary figure 9. Differentially expressed genes in Cas13bt3-VEGFA against**
1125 **Cas13bt3-NT.** Volcano plots from scRNA-seq for each retinal cell type showing differentially
1126 expressed genes between retinal organoid infected with Cas13bt3-VEGFA sgRNA and

1127 Cas13bt3-NT sgRNA. Significant downregulation of VEGFA in RPE cells is highlighted in
1128 red.

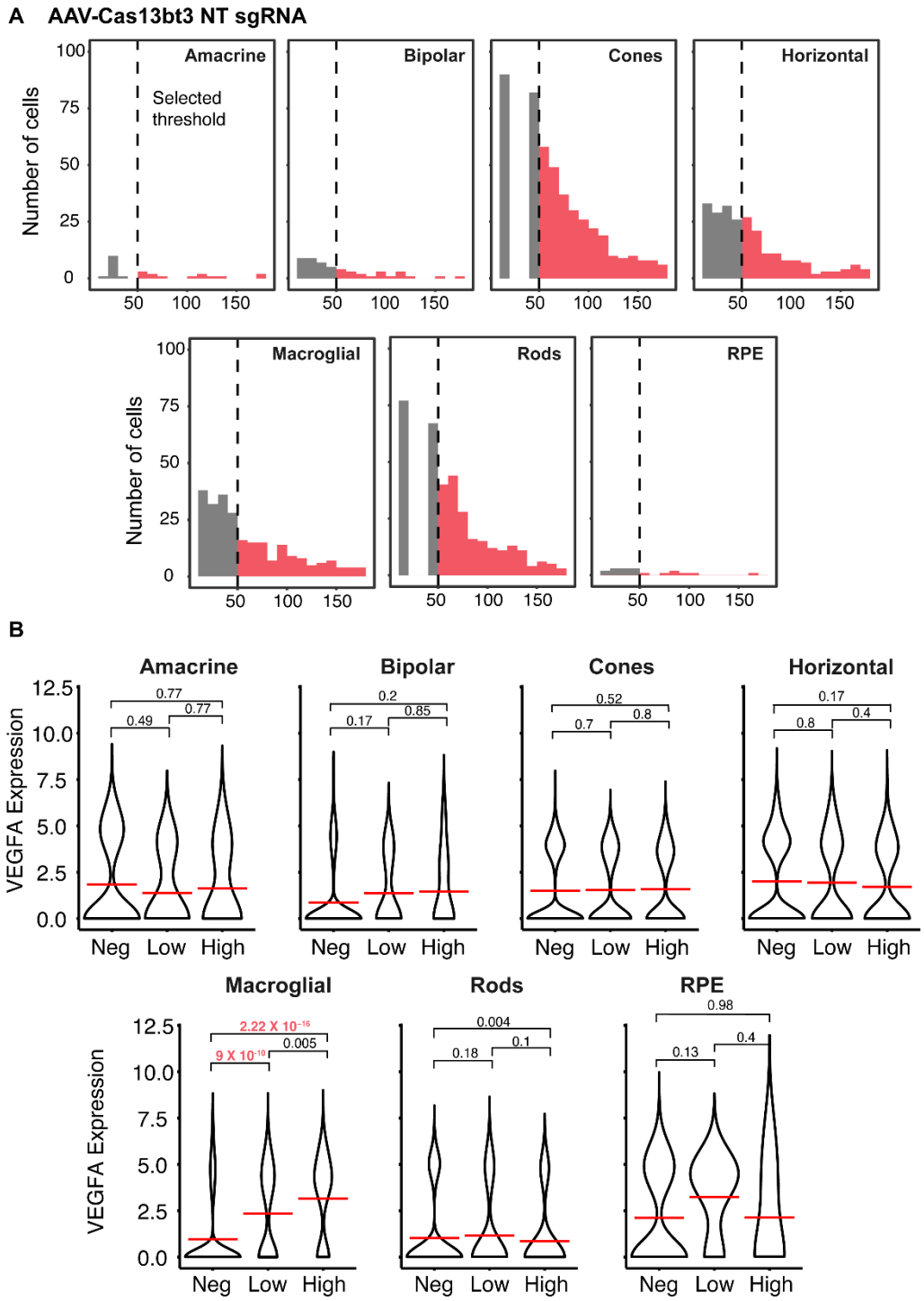

1129

1130 **Supplementary figure 10. Cas13bt3-NT sgRNA treatment in retinal organoids. (A)**
1131 Expression of Cas13bt3 by number of reads across retinal cell types in NT sgRNA treatment
1132 group. **(B)** Violin plots of VEGFA expression in cells with low and high expression of
1133 Cas13bt3 against Cas13bt3 negative cells showed no significant differences.

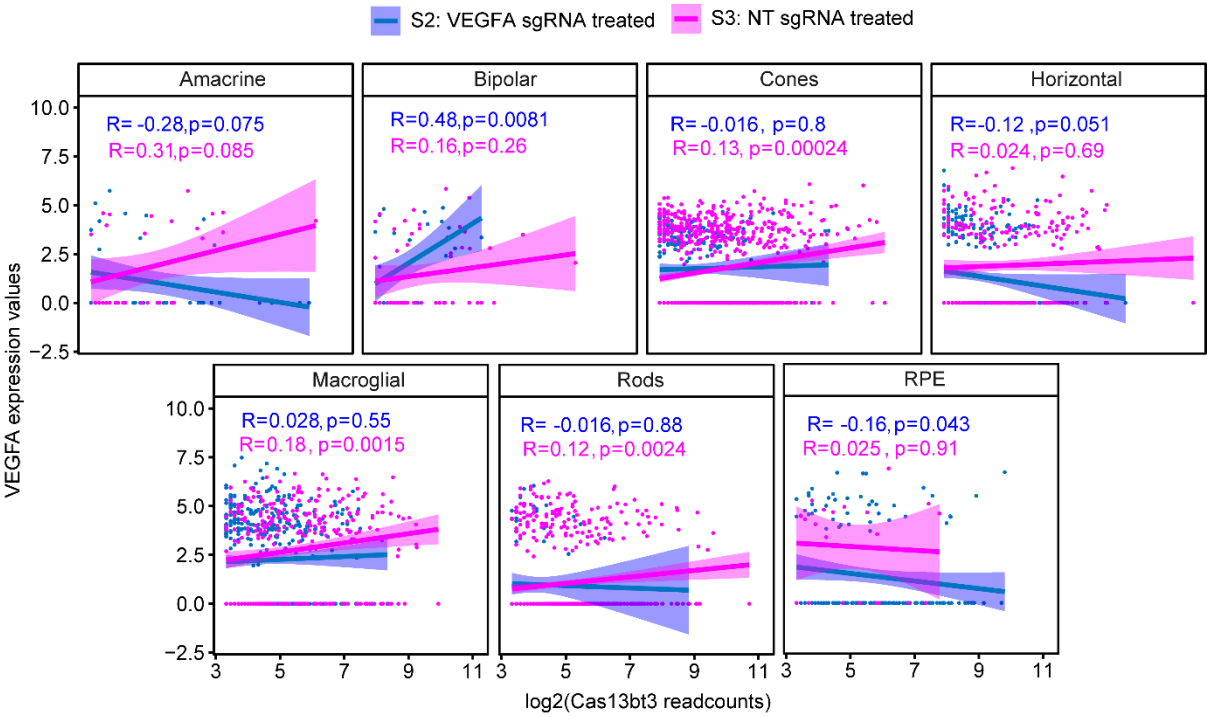

Supplementary figure 11. Expression of Cas13bt3 plotted against expression of *VEGFA* mRNA across cell types in NT sgRNA and VEGFA sgRNA groups.

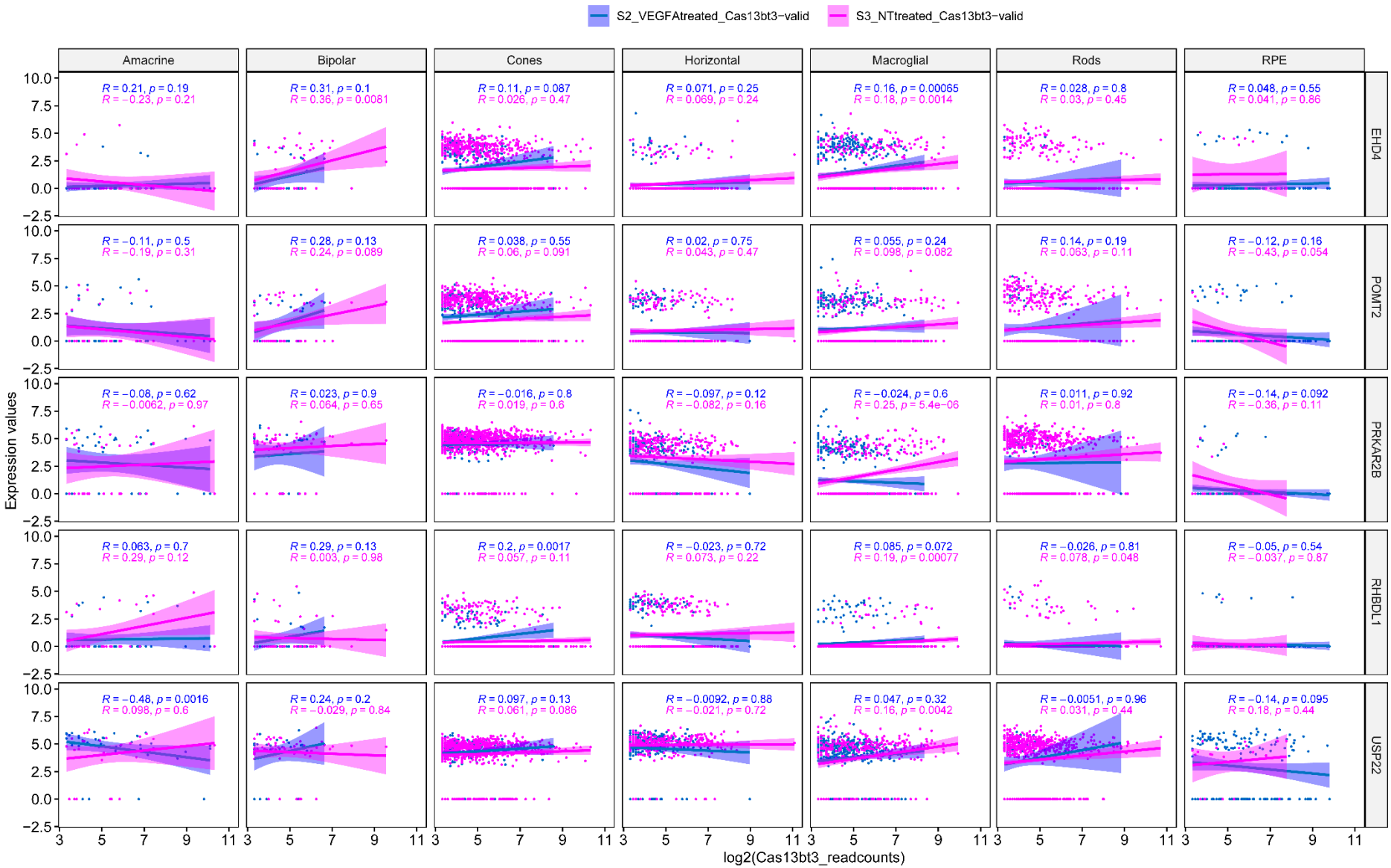
S2_VEGFAtreated_Cas13bt3−valid
S3_NTtreated_Cas13bt3−valid
Amacrine
Bipolar
Cones
Horizontal
Macroglial
Rods
RPE
EHD4
POMT2
PRKAR2B
RHBDL1
USP22
R = 0.21, p = 0.19
R = −0.23, p = 0.21
R = 0.31, p = 0.1
R = 0.36, p = 0.0081
R = 0.11, p = 0.087
R = 0.026, p = 0.47
R = 0.071, p = 0.25
R = 0.069, p = 0.24
R = 0.16, p = 0.00065
R = 0.18, p = 0.0014
R = 0.028, p = 0.8
R = 0.03, p = 0.45
R = 0.048, p = 0.55
R = 0.041, p = 0.86
R = −0.11, p = 0.5
R = −0.19, p = 0.31
R = 0.28, p = 0.13
R = 0.24, p = 0.089
R = 0.038, p = 0.55
R = 0.06, p = 0.091
R = 0.02, p = 0.75
R = 0.043, p = 0.47
R = 0.055, p = 0.24
R = 0.098, p = 0.082
R = 0.14, p = 0.19
R = 0.063, p = 0.11
R = −0.12, p = 0.16
R = −0.43, p = 0.054
R = −0.08, p = 0.62
R = −0.0062, p = 0.97
R = 0.023, p = 0.9
R = 0.064, p = 0.65
R = −0.016, p = 0.8
R = 0.019, p = 0.6
R = −0.097, p = 0.12
R = −0.082, p = 0.16
R = −0.024, p = 0.6
R = 0.25, p = 5.4e−06
R = 0.011, p = 0.92
R = 0.01, p = 0.8
R = −0.14, p = 0.092
R = −0.36, p = 0.11
R = 0.063, p = 0.7
R = 0.29, p = 0.12
R = 0.29, p = 0.13
R = 0.003, p = 0.98
R = 0.2, p = 0.0017
R = 0.057, p = 0.11
R = −0.023, p = 0.72
R = 0.073, p = 0.22
R = 0.085, p = 0.072
R = 0.19, p = 0.00077
R = −0.026, p = 0.81
R = 0.078, p = 0.048
R = −0.05, p = 0.54
R = −0.037, p = 0.87
R = −0.48, p = 0.0016
R = 0.098, p = 0.6
R = 0.24, p = 0.2
R = −0.029, p = 0.84
R = 0.097, p = 0.13
R = 0.061, p = 0.086
R = −0.0092, p = 0.88
R = −0.021, p = 0.72
R = 0.047, p = 0.32
R = 0.16, p = 0.0042
R = −0.0051, p = 0.96
R = 0.031, p = 0.44
R = −0.14, p = 0.095
R = 0.18, p = 0.44
Expression values
log2(Cas13bt3_readcounts)

1137

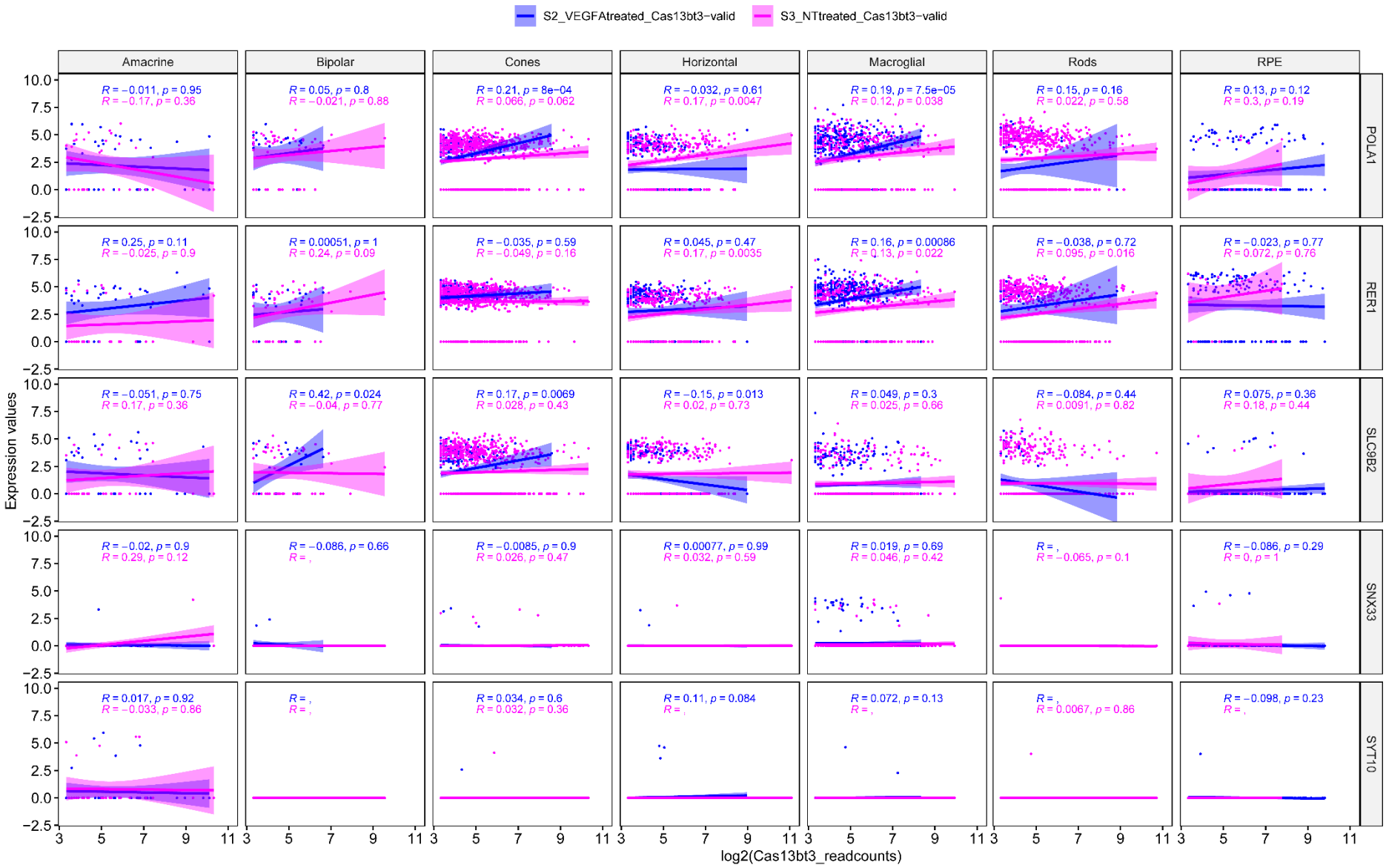
S2_VEGFAtreated_Cas13bt3−valid
S3_NTtreated_Cas13bt3−valid
Amacrine
Bipolar
Cones
Horizontal
Macroglial
Rods
RPE
POLA1
RER1
SLC9B2
SNX33
SYT10
R = −0.011, p = 0.95
R = −0.17, p = 0.36
R = 0.05, p = 0.8
R = −0.021, p = 0.88
R = 0.21, p = 8e−04
R = 0.066, p = 0.062
R = −0.032, p = 0.61
R = 0.17, p = 0.0047
R = 0.19, p = 7.5e−05
R = 0.12, p = 0.038
R = 0.15, p = 0.16
R = 0.022, p = 0.58
R = 0.13, p = 0.12
R = 0.3, p = 0.19
R = 0.25, p = 0.11
R = −0.025, p = 0.9
R = 0.00051, p = 1
R = 0.24, p = 0.09
R = −0.035, p = 0.59
R = −0.049, p = 0.16
R = 0.045, p = 0.47
R = 0.17, p = 0.0035
R = 0.16, p = 0.00086
R = 0.13, p = 0.022
R = −0.038, p = 0.72
R = 0.095, p = 0.016
R = −0.023, p = 0.77
R = 0.072, p = 0.76
R = −0.051, p = 0.75
R = 0.17, p = 0.36
R = 0.42, p = 0.024
R = −0.04, p = 0.77
R = 0.17, p = 0.0069
R = 0.028, p = 0.43
R = −0.15, p = 0.013
R = 0.02, p = 0.73
R = 0.049, p = 0.3
R = 0.025, p = 0.66
R = −0.084, p = 0.44
R = 0.0091, p = 0.82
R = 0.075, p = 0.36
R = 0.18, p = 0.44
R = −0.02, p = 0.9
R = 0.29, p = 0.12
R = −0.086, p = 0.66
R = ,
R = −0.0085, p = 0.9
R = 0.026, p = 0.47
R = 0.00077, p = 0.99
R = 0.032, p = 0.59
R = 0.019, p = 0.69
R = 0.046, p = 0.42
R = ,
R = −0.065, p = 0.1
R = −0.086, p = 0.29
R = 0, p = 1
R = 0.017, p = 0.92
R = −0.033, p = 0.86
R = ,
R = ,
R = 0.034, p = 0.6
R = 0.032, p = 0.36
R = 0.11, p = 0.084
R = ,
R = 0.072, p = 0.13
R = ,
R = ,
R = 0.0067, p = 0.86
R = −0.098, p = 0.23
R = ,
Expression values
log2(Cas13bt3_readcounts)

1138

1139 **Supplementary figure 12. Correlation plots of Cas13bt3 with VEGFA expression in the various retinal cell types for the predicted off-**
1140 **target genes of VEGFA sgRNA.**

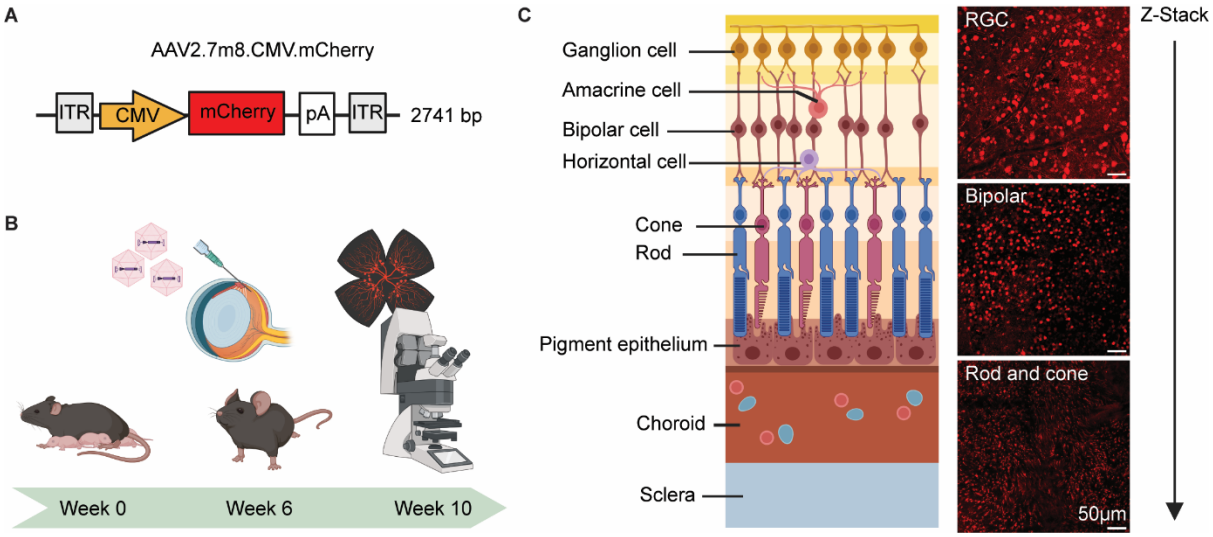

Supplementary figure 13. Intravitreal delivery of AAV2.7m8 achieves strong transduction of mice photoreceptors. (A) Schematic of AAV2.7m8 virus carrying mCherry reporter. **(B)** Schematic of experimental procedure for intravitreal injection of C57J/BL6 mice eyes. **(C)** Confocal microscope images of retinal flatmount 4 weeks post intravitreal injection, showing transduction of ganglion, bipolar, cone and rod cells with reference image of retinal cell layers.

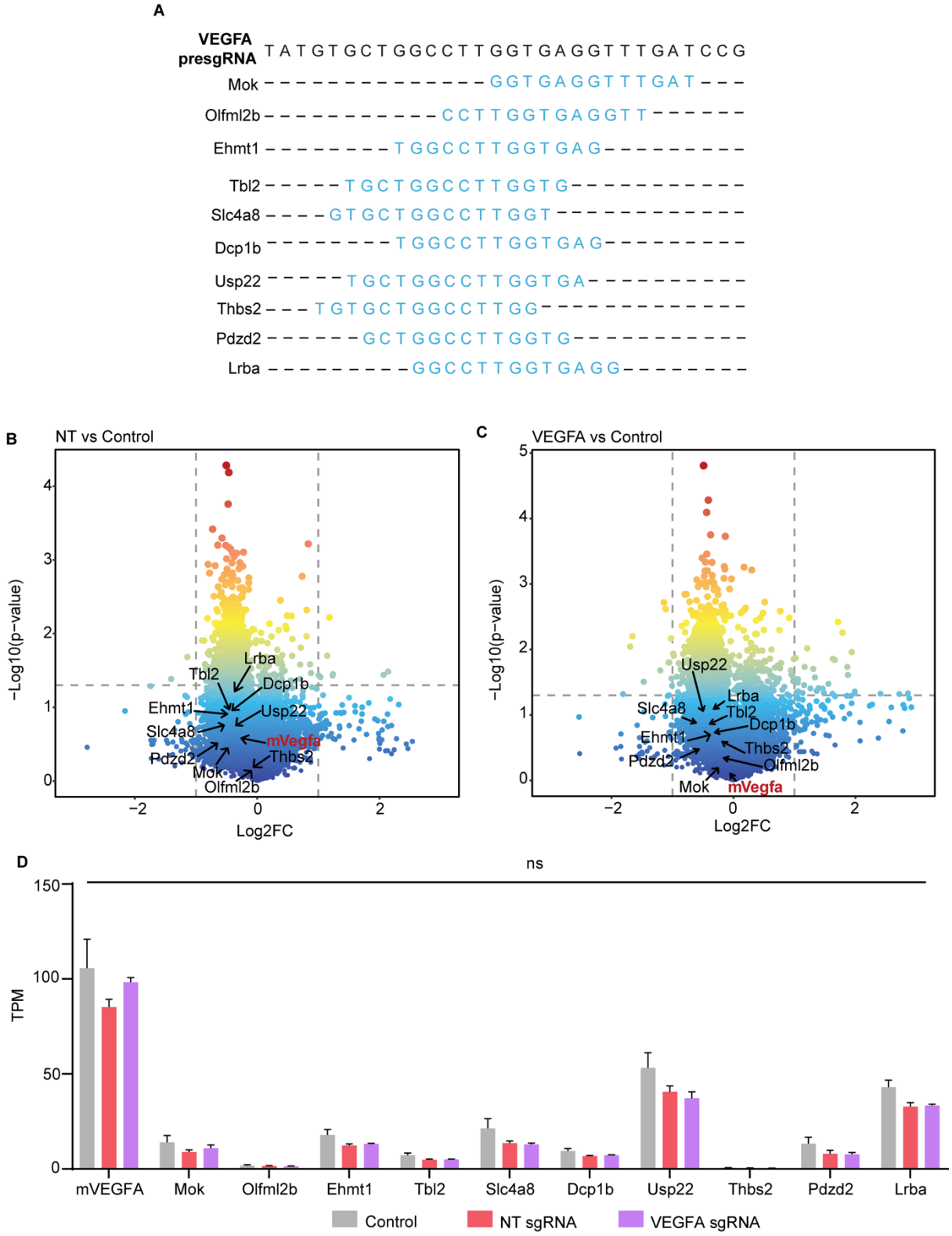

Supplementary Figure 14. Cas13bt3 off-target effects in Kimba mice. (A) Schematic of candidate off-target genes to VEGFA sgRNA in mouse transcriptome. Volcano plots of differentially expressed genes from Kimba mice retinas treated with AAV2.7m8 carrying **(B)**

Cas13bt3-NTsgRNA and **(C)** Cas13bt3-VEGFAsgRNA compared to vector controls. **(D)** Expression in TPM of mouse VEGFA and candidate off-target genes from RNA-seq.

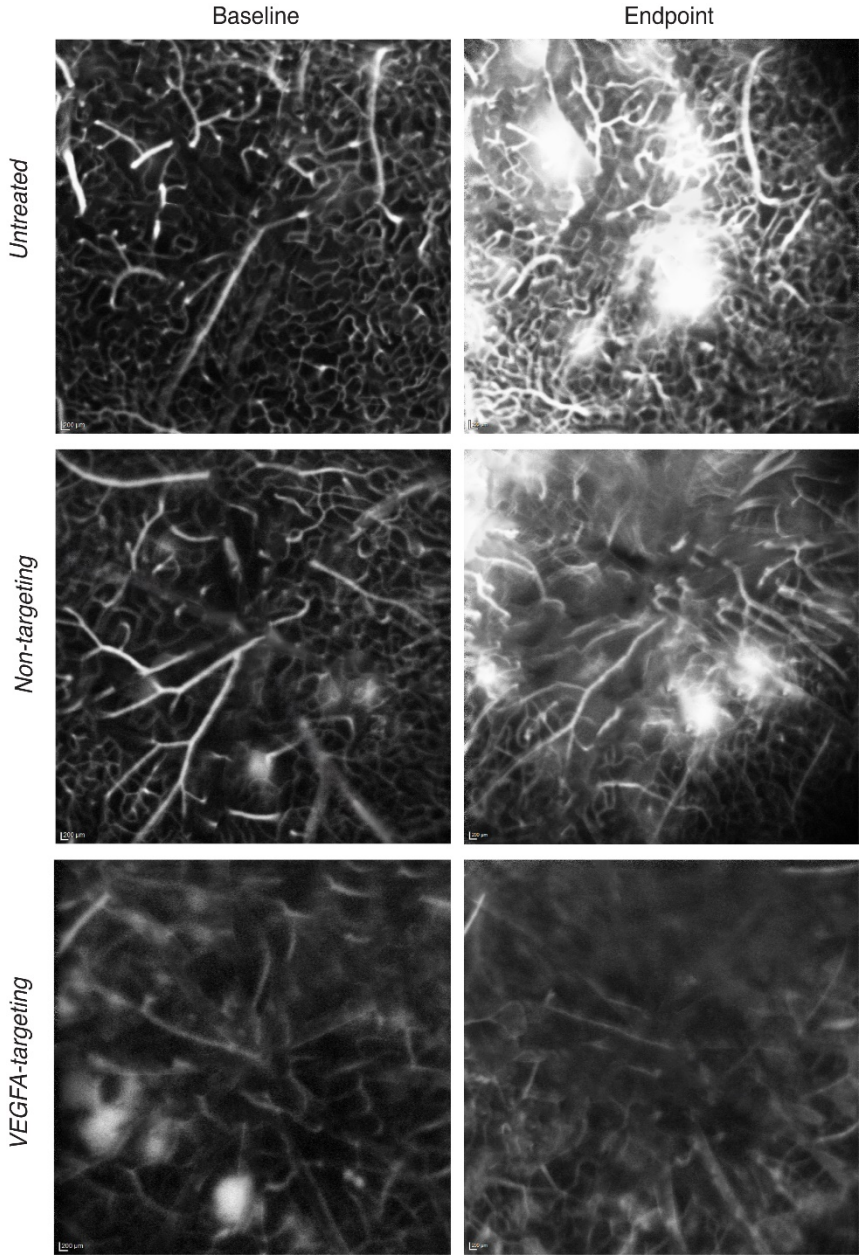

Supplementary figure 15. Original fundus fluorescein angiography images from Kimba mice retinae.

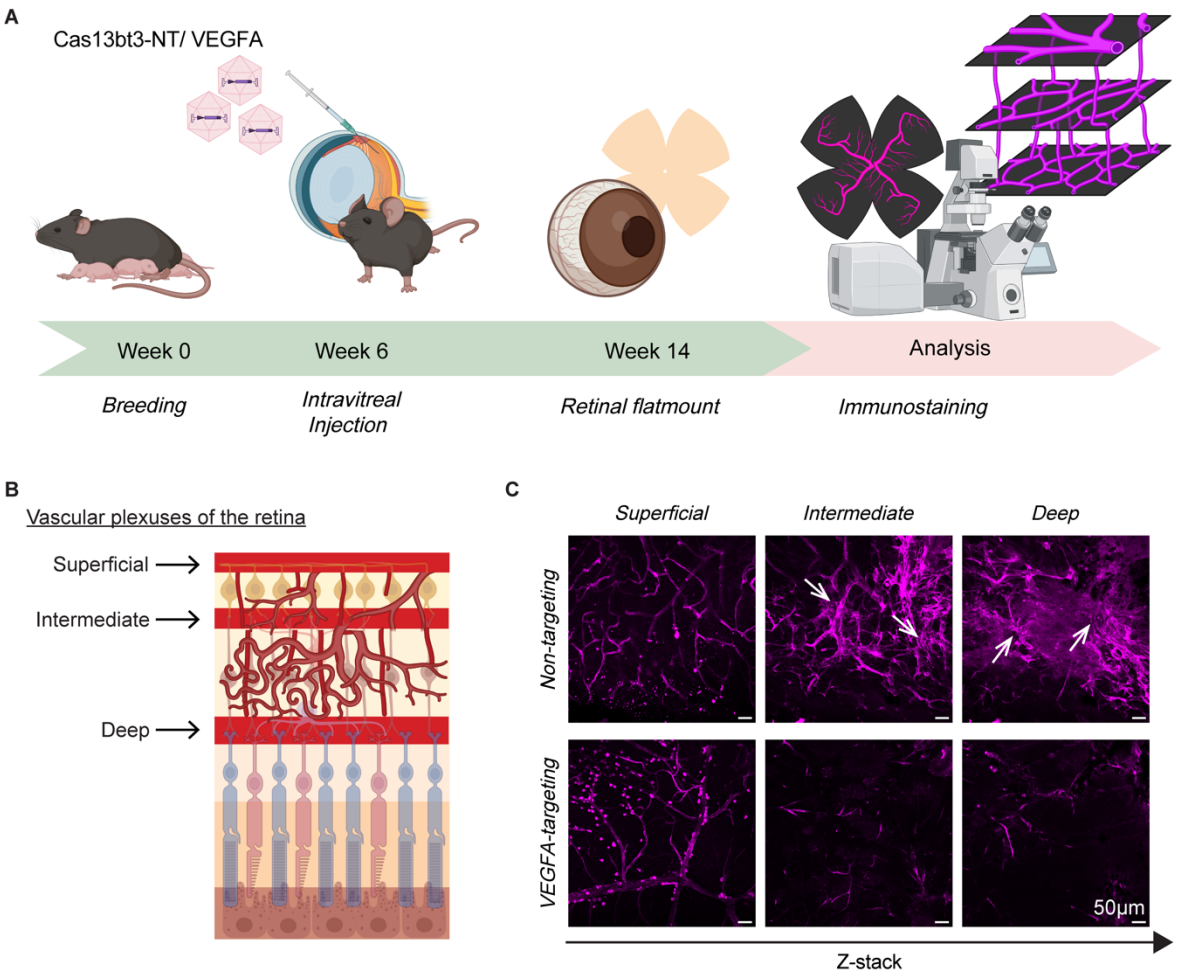

Supplementary figure 16. Imaging of retinal vascular plexuses Kimba mice treated with Cas13bt3-NTsgRNA and Cas13bt3-VEGFAsgRNA. (A) Schematic of experimental procedure for imaging retinal vascular plexuses. **(B)** Schematic of the different retinal plexuses. **(C)** Confocal imaging of the retinal plexuses, 8 weeks after Cas13bt3 treatment, immunolabelled with laminin. Magnification 40X, scale bar: 50µm. White arrows indicate leaky vessel structure.

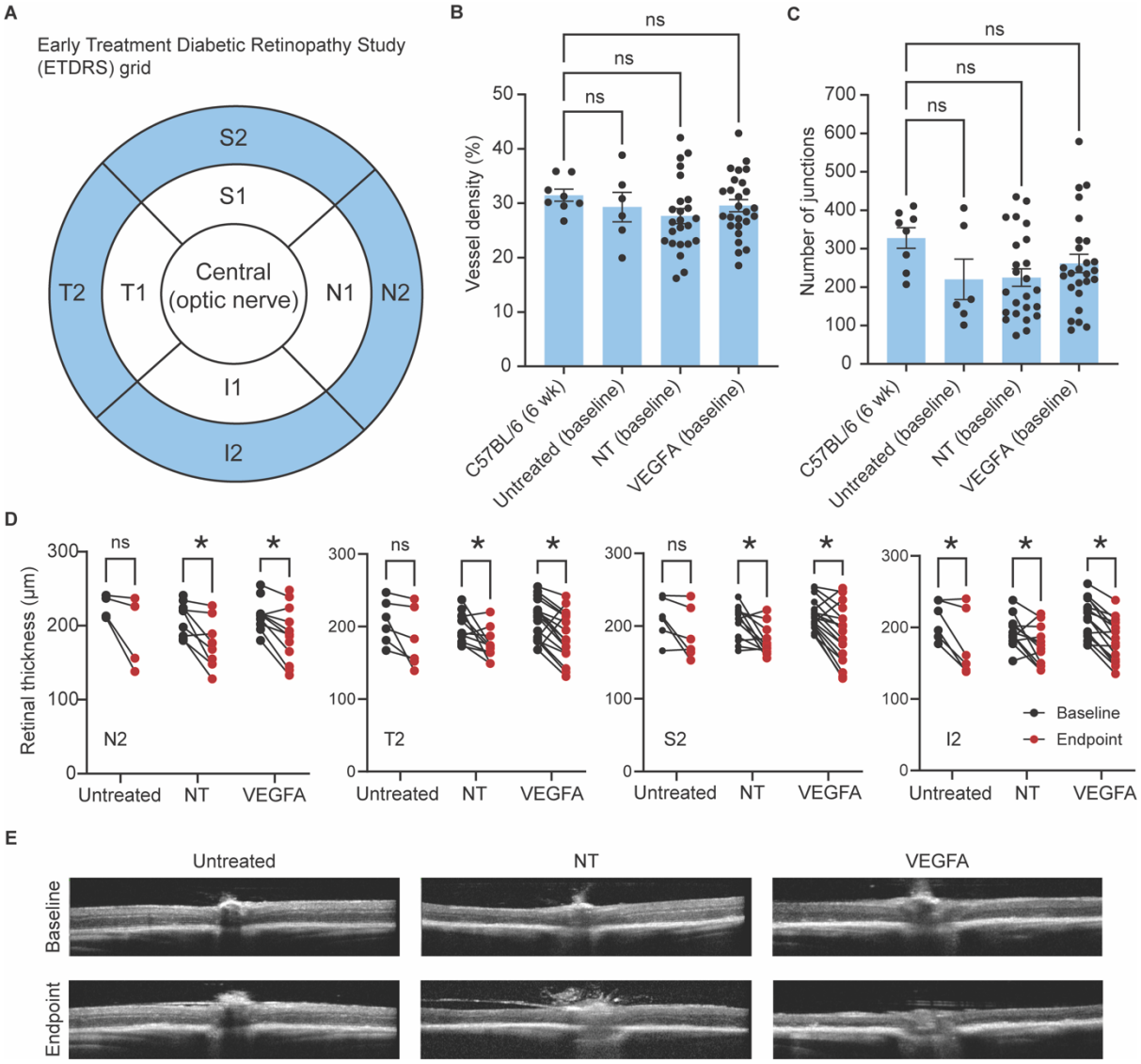

Supplementary figure 17. Retinal thickness readings from optical coherence tomography (OCT) in Kimba mice. (A) Early Treatment of Diabetic Retinopathy Study (ETDRS) grid showing segments of the retina analysed using OCT. C:Central (optic nerve); N1: Inner nasal; N2: Outer Nasal; T1: Inner temporal; T2: Outer temporal; S1: inner superior; S2: Outer superior; I1: Inner inferior; I2: Outer inferior. **(B)** Vessel density and **(C)** number of junctions readings from FFA images of Kimba mice at baseline compared to wildtype (C57BL/6) mice. **(D)** Plot of difference in total retinal thickness in untreated and treated Kimba mice between baseline and endpoint. **(E)** Representative OCT images from untreated and treated Kimba mice at endpoint.